Models of adsorption-induced deformation: ordered materials and beyond

A.L. Kolesnikov, 1, a) Yu.A. Budkov, 2, 3 and G.Y. Gor4

Adsorption-induced deformation is a change in geometrical dimensions of an adsorbent material caused by gas or liquid adsorption on its surface. This phenomenon is universal and sensitive to adsorbent properties, which makes its prediction a challenging task. However, the pure academic interest is complemented by its importance in a number of engineering applications with porous materials characterization among them. Similar to classical adsorption-based characterization methods, the deformation-based ones rely on the quality of the underlying theoretical framework. This fact stimulates the recent development of qualitative and quantitative models toward the more detailed description of a solid material, e.g. account of non-convex and corrugated pores, calculations of adsorption stress in realistic three-dimension solid structures, the extension of the existing models to new geometries, etc. The present review focuses on the theoretical description of adsorption-induced deformation in micro and mesoporous materials. We are aiming to cover recent theoretical works describing the deformation of both ordered and disordered porous bodies.

¹⁾ Institut für Nichtklassische Chemie e.V., Permoserstr. 15, 04318 Leipzig, Germany

²⁾ School of Applied Mathematics, Tikhonov Moscow Institute of Electronics and Mathematics, HSE University, Tallinskaya St. 34, 123458 Moscow, Russia

³⁾G.A. Krestov Institute of Solution Chemistry of the Russian Academy of Sciences, Academicheskaya St., 1, 153045 Ivanovo, Russia

⁴⁾Otto H. York Department Chemical and Materials Engineering, New Jersey Institute of Technology, University Heights, Newark, NJ 07102, USA

 $^{^{\}mathrm{a})}$ kolesnikov@inc.uni-leipzig.de

I. INTRODUCTION

Adsorption-induced deformation (AID) is a change in geometrical dimensions of an adsorbent material caused by gas or liquid adsorption on its surface. AID is typically quantified experimentally by a deformation/strain isotherm, which is similar to an adsorption isotherm (see Fig.1 for details), i.e. the dependence of material deformation on relative or absolute pressure of an adsorptive. AID phenomenon is universal although the magnitude depends on many factors: adsorbent-adsorbate interactions, pore geometry, adsorbent elastic constants and porosity, surface-to-volume ratio, etc. Thus, it is clear, that there is no unique pattern of strain isotherm for diverse porous materials. Most adsorbent-adsorbate pairs show monotonic expansion with the increase of adsorbate pressure¹⁻³, some show monotonic contraction⁴⁻⁶, other behave non-monotonically, contracting at low pressures, and expanding at higher pressures. The anisotropic nature of AID additionally complicates the classification of strain isotherms, they cannot be easily reduced to a single scalar parameter (as adsorbed amount for adsorption isotherms, for instance). Deformation magnitude also varies a lot depending on the material properties from fraction up to tens of percents. The latter, in general, is observed in polymers⁷, aerogels^{8,9}, and metal-organic frameworks (MOFs)¹⁰.

MOFs are a subclass of soft porous crystals, exhibiting structural deformations due to various external stimuli. These include temperature¹¹, external mechanical force¹², light^{13,14}, electric field¹⁵, guest adsorption^{16,17}, etc. Adsorption-induced deformation in MOFs has outstanding characters, which are not observed in more common porous materials like silica and carbon. Guest-host interactions could lead to a structural transition of the host material, in contrast to "simple" swelling/shrinkage discussed above. In addition, the deformation does not necessarily cause a volume change¹⁸, for example, rotation of an organic linker can be done at a constant volume. In this review, we will narrow down the broad area and focus on the deformations accompanied by volume change, which include "breathing" and "gate opening". Gate opening can be described as a sharp transition from a nonporous to porous host induced by adsorption of guest molecules. Breathing is a more complex process consisting of a series of adsorption-induced transitions between different structures. A particular material possessing such a deformation type is MIL-53. Its structure can oscillate between large pore (lp) and narrow pore (np) with a cell volume difference between them around 38 % ¹⁹.

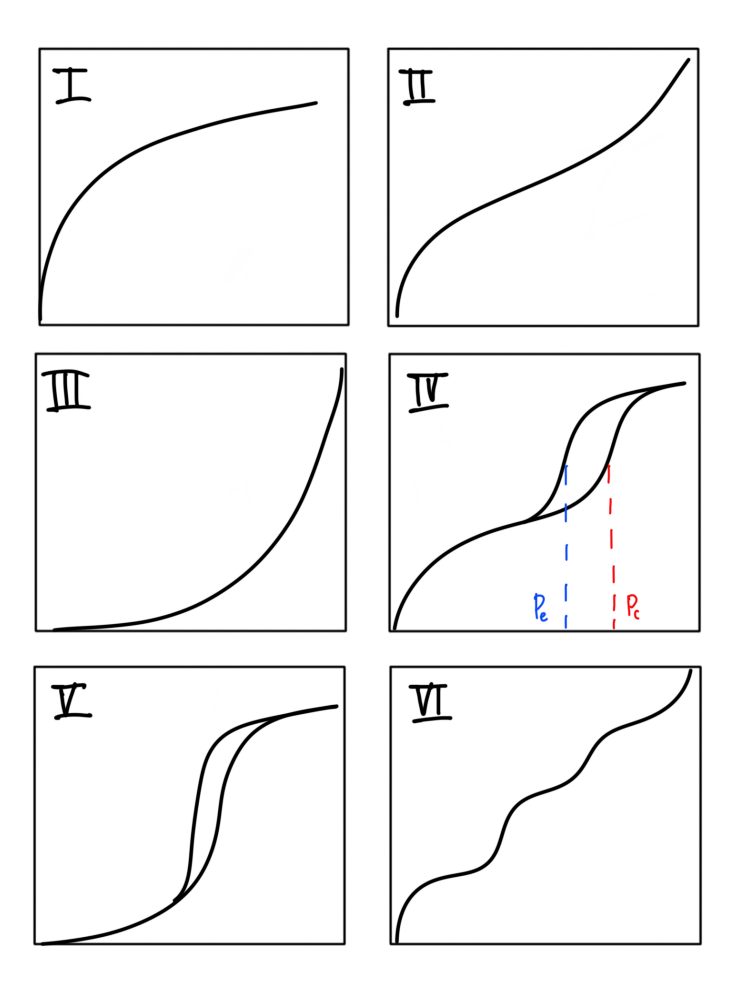


Figure 1: Types of adsorption isotherms 20,21 . Type I isotherms corresponds to the microporous solids with strong adsorbent-adsorptive interactions; type II corresponds to the physisorption on nonporous or macroporous adsorbents; type III isotherms are given by nonporous or macroporous solids with weak adsorbent-adsorptive interactions; type IV isotherms are typical for mesoporous solids with strong adsorbate-adsorptive interactions, on the other hand type V can be attributed to relatively weak adsorbate-adsorptive interactions; type VI corresponds to a stepwise adsorption on a uniform and nonporous surface. Types IV and V have a hysteresis loop associated with fluid condensation in a pore. Here we denoted by $p_{\rm c}$ approximate position of capillary condensation on the adsorption branch of the isotherm and by $p_{\rm e}$ approximate position of capillary evaporation, which happens during a desorption process.

Nowadays, several possible areas of applications of adsorption-induced deformation have been discussed in the literature: sensors^{22–24}, actuators^{25,26}, characterization of porous materials^{27–30}. Most of the proposed sensors and actuators are based on the same principle, namely usage of the strain gradient arising from the inhomogeneity of the material with respect to the guest molecules binding. In Ref.24 the authors used an "artificial nose" consisting of an array of microcantilevers. Differentiation of different molecules can be achieved by modification of a bare cantilever with specific coating material, creating interactions sites for the target molecule. The difference between number of binding molecules of both sides of the cantilever results in its bending. The magnitude of the deformation is not of prime interest, unlike the sensitivity to minor changes of the concentration of the linked molecules. Their range could be quite broad, for instance, the response was demonstrated on the cancer detection³¹. On the other hand, actuation purpose requires large deformation magnitudes. As an example, we consider a concept proposed in the Ref.23. The authors demonstrated the humidity-induced deflection of a mesoporous silica/nonporous silicon bilayer. The working principle is similar to the discussed above, i.e. much more pronounced adsorption-induced deformation of a mesoporous silica layer in comparison to a nonporous silicon layer results in the overall bending of the material.

Adsorption-induced deformation can be applied for the characterization of porous materials also. One can identify two possible strategies: obtaining an elastic constant from strain isotherm and/or its usage for determination of pore size distribution (PSD). The first case was demonstrated by Mogilnikov and Baklanov³² by example of mesoporous low-k film. The elastic constant was obtained from the part of the strain isotherm corresponding to filled pores, where it is mostly defined by the capillary pressure. The same idea was also discussed in Refs.³³ in the context of mesoporous materials, which is explained by the ease of the method. The second one is based on the usage of strain information in PSD determination. In Refs.^{29,34} the authors demonstrated that the mean pore size and the degree of polydispersity of PSD which can be obtained from a beam bending experiment in combination with nonlocal density functional theory (NLDFT) of solvation pressure calculations. Authors' modeling showed that stress response of the film is sensitive to the pore size distribution used in the calculations. The particular measurements and calculations were performed for microporous silica film. Similar ideas were expressed by Do and Ustinov³⁵, where they suggested that an experimental strain isotherm contains information on the PSD of the

material. Ref. 27 shows that strain isotherms are potentially more sensitive to the PSD determination than adsorption isotherms. Moreover, in ordered mesoporous materials, the average pore size and width of the PSD can be estimated from strain isotherm data without involving the adsorption isotherm³⁶.

When it comes to the theoretical predictions of adsorption-induced deformation, the two important aspects should be mentioned: thermodynamical and mechanical. The first one related to the source of deformation, i.e. defines the driving force (solvation pressure or disjoining pressure). As far as we are considering the complex fluid/solid system, it depends on the full set of intermolecular interactions, pore geometries, their connectivities, and environmental conditions. Thus, the particular microscopic mechanism is system-dependent. The second aspect should be taken into account when one wants to predict the solid response to the solvation pressure. It also requires the knowledge of intermolecular interactions of solid, pore network, and additional considerations on the deformation mechanism. The rigorous theoretical model should take into account the interconnection between both aspects, i.e. coupling between adsorption and deformation³⁷. However, when the deformation magnitude is low it is reasonable to estimate the solvation pressure in the undeformed solid body and predict the strain separately.

The present review focuses on to the theoretical description of adsorption-induced deformation in micro and mesoporous materials. Thus, we are not aiming to cover the experimental and computer simulation methods. The detailed literature review, which covers classical models and also experimental works, has been already published several years ago¹, so here we focus on recent results and describe the selected theoretical works in more detail. The review is divided into three parts: in the first one we describes the models developed for materials with a certain pore size and geometry, then we discuss generalizations of some of these models for materials with a pore size distribution. The final part describes the models in which the pore geometry/size cannot be unequivocally defined.

II. MODELS OF ORDERED MATERIALS

Most of the theoretical approaches aiming to describe adsorption-induced deformation are based on the analysis of the following thermodynamic potential:

$$\Delta G = F_{\rm s} + \Omega + pV_{\rm s},\tag{1}$$

where F_s is the free energy of a solid material, Ω is the grand thermodynamic potential (GTP) of adsorbed fluid/gas phase, p is the surrounding (or bulk) pressure and V_s is the solid volume. The thermodynamic potential ΔG named differently by different authors: grand thermodynamic potential³⁵, osmotic potential¹⁹, solvation Gibbs free energy³⁶, etc. The latter is introduced by the analogy with the solvation thermodynamics³⁸ and here defines the difference between the Gibbs free energy of the system consisting of adsorbent in a huge reservoir of adsorbate and the Gibbs free energy of the reservoir solely. In our opinion, as far the difference is taken at a fixed temperature and adsorbate pressure the term "solvation Gibbs free energy" is the most appropriate one (however, ΔG is also equal to the corresponding change of the Helmholtz free energy in the process performed at a fixed temperature and adsorbate number of particles — it follows from the small addition theorem³⁹). We denote it as ΔG , to avoid a potential confusion with the Gibbs free energy. It should be noted that here we consider only systems, in which the external stress on a solid is defined by the fluid pressure. There are two ways to calculate Ω , one is through the equation:

$$\left(\frac{\partial\Omega}{\partial\mu}\right)_{VT} = -N\tag{2}$$

and another is based on the construction of the GTP within the framework of equilibrium statistical physics. Below we discuss the models of adsorption-induced deformation in ordered materials with different degrees of coupling between adsorption and deformation processes.

A. Models with no host response: slit pore geometry

One of the first comprehensive studies of solvation force was done by Balbuena et al^{40} . The system was defined as a Lennard-Jones (LJ) fluid confined between the two semi-infinite parallel walls. The authors studied the influence of temperature, pore width, and LJ parameters ($\epsilon_{\rm ff}$ and $\sigma_{\rm ff}$) by means of nonlocal mean-field density functional theory based on Tarazona's approximation⁴¹. The particular examples, which we took for the present review, were calculated for methane with the Steele potential⁴² representing the solid-fluid interactions⁴³. The NLDFT was used for the calculation of the density profile, while the

adsorption stress was calculated as its derivative⁴⁰:

$$P_{\rm s,slit} = -\frac{1}{S} \left(\frac{\partial \Omega}{\partial H} \right)_{T,\mu} = -\int_{-\infty}^{\infty} dz \rho(z) \left(\frac{\partial V_{\rm ext}(z, H)}{\partial H} \right), \tag{3}$$

where S is half the surface area of a pore and $V_{\rm ext}(z,H)$ is the external potential of solid-fluid interactions depending on z coordinate and width, H, of the pore. For the slit pore geometry solvation pressure is equal to the difference between the adsorption stress and the pressure in the reservoir, i.e. $f = P_{\rm s} - P$ and can be called disjoining pressure⁴⁴. As one can see, the planar geometry allows us to express solvation pressure as a functional of density profile. This equation underlines the complexity of the analysis, because both $\rho(z)$ and $\partial V_{\rm ext}/\partial H$ depend on the LJ parameters and solid-fluid interaction potential.

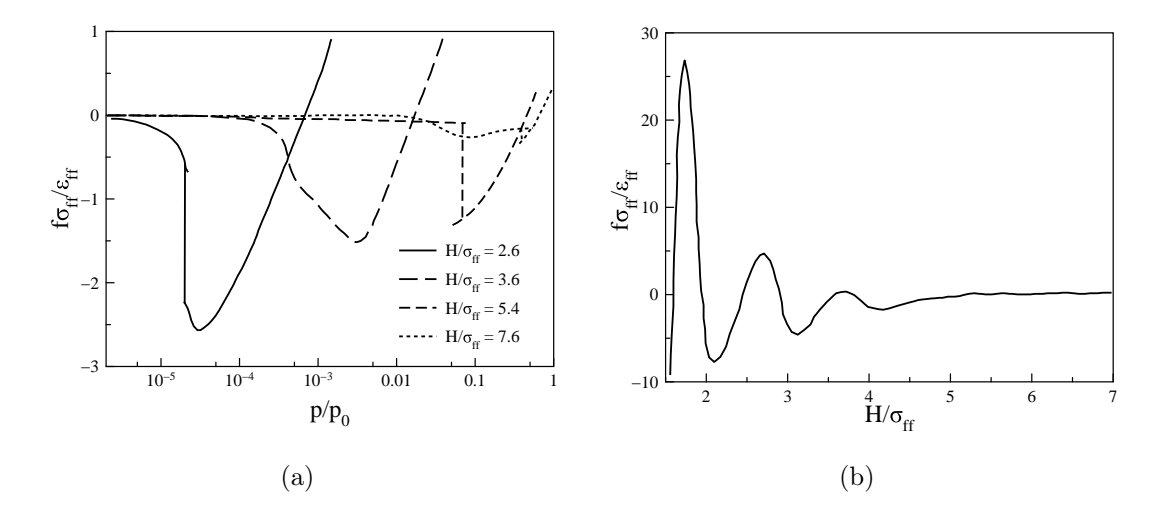


Figure 2: (a) Solvation pressure isotherms as a function of relative pressure for 0.9 nm, 1.37 nm, 2.06 nm and 2.9 nm slit pores at $k_{\rm B}T/\epsilon_{\rm ff}=0.8$. (b) Solvation pressure for methane as a function of pore width H for the fixed bulk density $\rho\sigma_{\rm ff}^3=0.005$ at $k_{\rm B}T/\epsilon_{\rm ff}=1.1$. Data is taken from Ref.40.

Fig. 2 (a) demonstrate the adsorption induced solvation pressure for several pores with different width (0.9 nm, 1.37 nm, 2.06 nm and 2.9 nm) at a fixed temperature. All of the curves show qualitatively similar behavior. At low vapor pressure $P_{\rm s,slit} \to 0$, it remains negative and increases in magnitude with the increases in adsorptive pressure. At higher vapor pressures, $P_{\rm s,slit}$ goes through a minimum and becomes positive. The solvation pressure exhibits oscillations when it is plotted as a function of pore width (see, Fig. 2 (b)).

Their usual interpretation is based on the fluid packing effect in the small pores. Thus, the maxima correspond to the more dense adsorbed phase in comparison to the minima. Higher temperature and larger pore width damp the magnitude of the oscillations. The works^{28,45} demonstrate qualitatively different dependence on relative pressure in microporous in addition to described above. Gregoire et al. 45 calculated a map of methane solvation pressure for slit micropores at 373 K and bulk pressure from 0 to 200 bar. The calculations were performed via density functional theory based on SAFT-VR (statistical associating fluid theory with attractive potentials of variable range)⁴⁶ equation of state. The map demonstrates three qualitatively different behaviors of $P_{\rm s,slit}$ on relative pressure, namely monotonic increase, monotonic decrease, and non-monotonic regime with a minimum. Similar results were obtained by Balzer et al.²⁸ for argon, nitrogen, and carbon dioxide within the fundamental measure theory (FMT) based DFT with mean-field treatment of attractive interactions. Thus, the non-local DFT, probably regardless of the particular treatment of short and long-range interactions, reproduces the non-monotonic behavior of solvation force similar to experimental data⁴⁷. This fact is crucial for the applications of adsorption-induced deformation, namely PSD determination from a strain isotherm. We will continue the discussion in the second section of the review.

B. Models with no host response: cylindrical pore geometry

Cylindrical pore geometry is one of the most common approximation in the field of material characterization⁴⁸. Some materials have pores which can be modeled as perfect cylinders with a good accuracy, for instance templated mesoporous silica materials (MCM-41, SBA-15). Gor and Neimark⁴⁹ proposed a model of adsorption-induced deformation of mesoporous materials with cylindrical pores. It is based on the Derjaguin-Broekhoff-de Boer (DBdB) theory of capillary condensation, which has established itself as a very accurate tool^{50,51}. The adsorption process is presented as a growth of a liquid-like film on the pore surface, which is, by means of capillary condensation, fills the entire pore (see, Fig. 1 in the Introduction, namely Type IV isotherm). The properties of the film are assumed to be equal to the liquid ones at the binodal at the same temperature. As far as the model decouples the adsorption and deformation processes the positions of capillary condensation/evaporation

were inherited from DBdB theory. The adsorption-induced stress was defined as⁴⁹:

$$P_{\rm s,cyl} = -\frac{1}{S_{\rm cyl}} \left(\frac{\partial \Omega}{\partial R}\right)_{\mu,T},\tag{4}$$

where $S_{\rm cyl}$ is the surface area of the pore and R is the radius of cylinder. The deformation model $f_{\rm cyl} \approx K\epsilon_{\rm vol}$ assumes the linear dependence of solvation pressure on the volumetire strain, $\epsilon_{\rm vol}$. K is an effective elastic modulus of the porous material, which should not be mistaken with an elastic modulus of pore walls⁵². Grand thermodynamic potential Ω was calculated by the equation (2) for the two regimes — film adsorption and filled pore and thereby leads to the two equations for solvation pressure. The general pattern of the solvation pressure dependence on the relative pressure is similar to one obtained for slit pores. However, the model⁴⁹ only predicts the swelling of the material at low pressures with the typical shrinkage during capillary condensation. The comparison with experimental data^{2,33} demonstrates the correct behavior right before and after the capillary condensation. The comparison with a more sophisticated approach (quenched solid density functional theory⁵³) shows that for cylindrical pores with diameter 4 nm and above both methods give similar results⁵⁴ (Fig. 3).

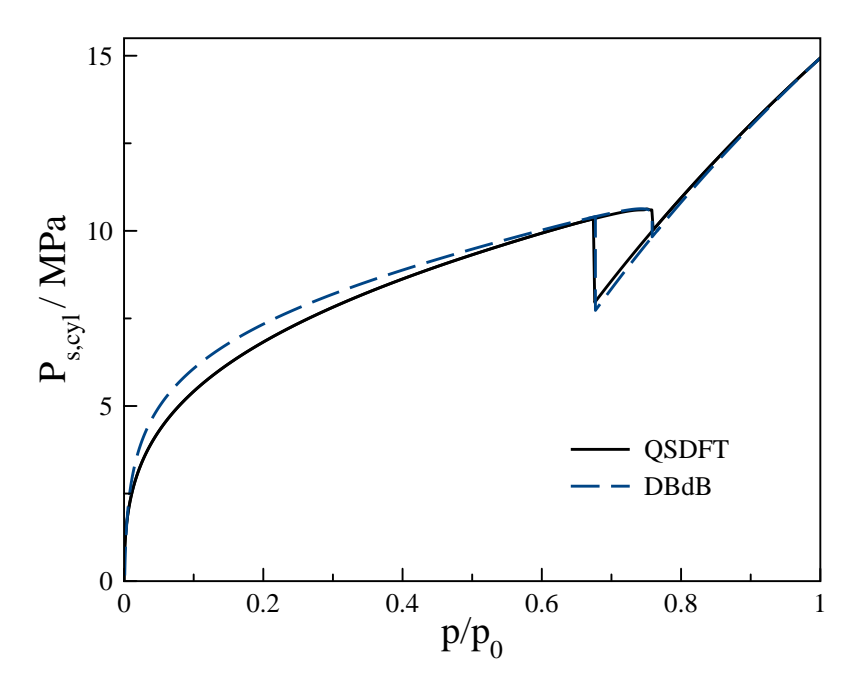


Figure 3: Solavtion pressure as a function of relative pressure for 8.2 nm cylindrical pore.

The calculations were performed via DBdB-based model and QSDFT.⁵⁴.

Our recent work generalized the predictions of adsorption-induced deformation from materials with ideal cylindrical pores to corrugated pores⁵⁵. We focused on the influence of capillary bridge formation on the AID at sub and supercritical temperatures. In both cases, the calculations were performed for nitrogen at 77 K and 154 K respectively. A unique part of the pore is presented in Fig. 4 as well as the schematic representation of different adsorbed phases. The elastic part of the model is based on the assumption, that the whole sample undergoes only volumetric deformations on the large scale (much greater than the typical pore size). This assumption could be reasonable for disordered materials, like glasses, where there is no predominant pore orientation in the whole material. Using the method from Ref.56, elastic free energy was represented in a Hooke's law like form with respect to an order parameter - average pore size. The adsorption stress was obtained proportional to the derivative of GTP⁵⁵:

$$P_{\rm s,corr} = -\frac{R_{\rm m}}{2\pi l_{\rm c}(R_{\rm m}^2 + \sigma^2)} \left(\frac{\partial \Omega}{\partial R_{\rm m}}\right)_{\mu,T},\tag{5}$$

with Ω being the GTP of the unique part of the pore; $R_{\rm m}$, $l_{\rm c}$, and σ are defined in Fig. 5 caption. In the absence of corrugations Eq. (5) transforms into the earlier defined solvation pressure for cylindrical pore. Also, within the proposed approach, we obtained that the deformation of the materials governed by different elastic constants in the cases when the force applied to the external and internal surfaces of the samples.

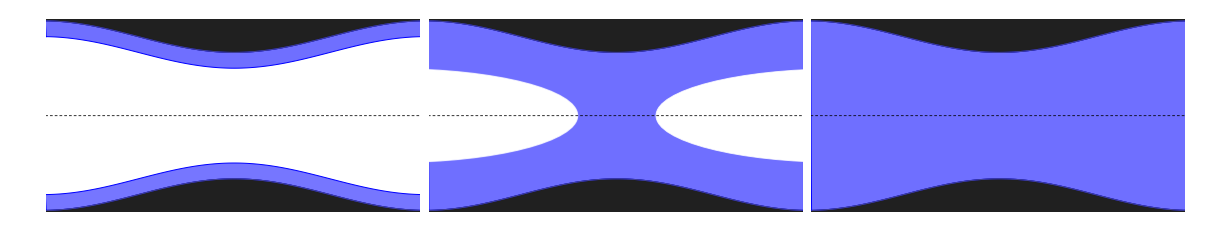


Figure 4: Schematic representation of adsorption process in the corrugated pore. Multilayer adsorption, capillary bridge formation, and completely filled pore are presented from left to right. A unique part of the corrugated pore defined by the equation $R_{\rm p}(z) = R_{\rm m} + \sqrt{2}\sigma\cos(2\pi z/l_{\rm c}); \ l_{\rm c} \ \text{is the corrugated length, } \sigma \ \text{is a parameter defining the corrugation amplitude, and } R_{\rm m} \ \text{is an average pore radius.}$ The dotted line denotes the pore axis. Data is taken from Ref.55

We used the theoretical description of the GTP based on the modification of DBdB theory for the corrugated pores proposed earlier by Gommes⁵⁷. The used GTP was composed as

a sum of three contributions: Ω_{film} — the GTP of the liquid-like film on the surface, Ω_{vapor} — the GTP of the remaining vapor phase in the pore and the excess contribution due to liquid-vapor interface between them. The local density functional theory was used for both volume contributions, however sub- and supercritical temperatures were treated separately. At the subcritical temperature incompressible approximation was used. On the other hand, at the supercritical temperature, compressibility was taken into account using van der Waals equation of state.

We calculated adsorption stress and adsorption isotherms for four different corrugation lengths at fixed corrugation amplitude. At the lowest value of l_c adsorption and stress isotherms in corrugated pore are very similar to ones in cylindrical pore. The exception is mainly the hysteresis loop which becomes narrower in the corrugated pore. The increase in l_c leads to the liquid bridge formation on both adsorption and stress isotherms (see, Fig. 5). Its effect on the stress isotherms is similar to the capillary condensation ones, i.e. the condensation or formation of a liquid bridge corresponds to the drop of solvation pressure. Adsorption stress generally increases during further bridge development. The further increase of corrugated length leads to the formation of two independent hysteresis loops. At sufficiently large l_c adsorption stress in the bridge regime goes through the maximum, which is correlated with a steep increase of the adsorption isotherm. All these effects disappear at the supercritical temperature and both cylindrical and corrugated pores demonstrate very similar behavior.

A possible candidate for such material could be SBA-15, whose complex porosity was studied experimentally by means of electron tomography^{58,59}. The authors obtained the inhomogeneities along the pore axis with corrugated length approximately 5 nm. Also, in Ref.60 the authors observed the periodic formation of nanobubles in the SBA-15 pores. Larger corrugation length was obtained, approximately 11 nm, which can be due to the different synthesis scheme. Both of these values are a bit lower than the values at which the capillary bridge formation occurs, but quite close to them.

Thus, we can conclude, that the models of adsorption-induced deformation based on the DBdB model are capable to predict the adsorption stress with good accuracy (in comparison with microscopic DFT models). Also, due to their relative simplicity, they can be extended to the pore geometries which are different from simple ones, at the same time the computation cost remains low.

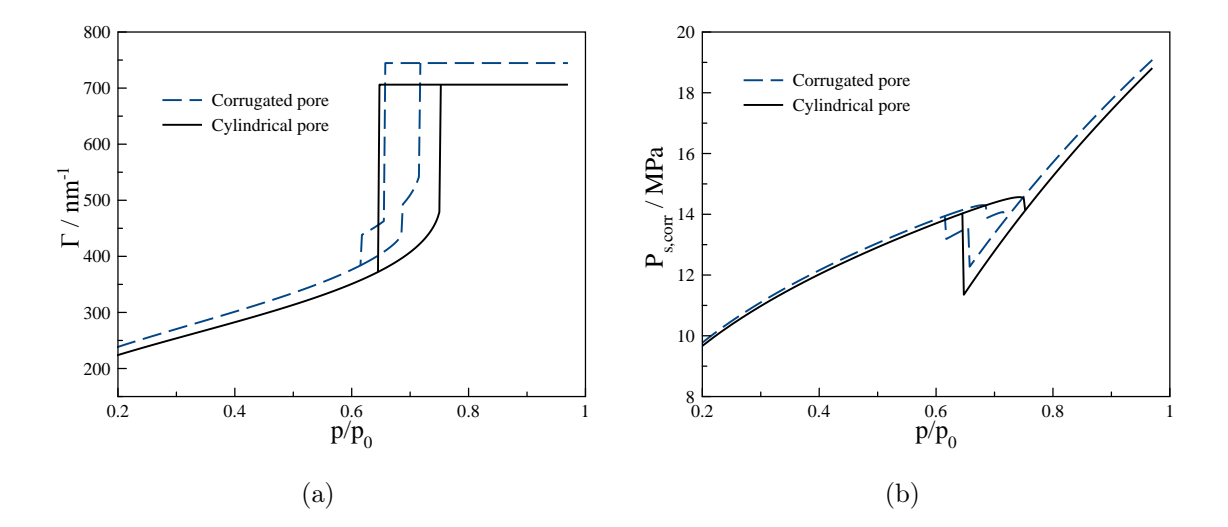


Figure 5: Adsorption and stress isotherms as a functions of relative pressure for cylindrical and corrugated pores, $l_c = 14 \,\mathrm{nm}$. In contrast to the cylindrical pores, corrugated ones demonstrate the capillary bridge formation on both adsorption and desorption branches of the isotherm. The adsorption stress behaves similarly during capillary condensation and bridge formation, i.e. abrupt decrease at the transition point. Data is taken from Ref.55.

C. Models with no host response: spherical pore geometry

In Ref.53 Ravikovitch and Neimark developed a model of adsorption-induced deformation of the material with spherical pores. The theoretical description is based on a number of assumptions, such as: isotropic deformation which can be characterized by a volumetric strain according to the Hooke's law, the density of solid matrix does not change and the deformation does not affect the adsorption process. The authors demonstrated that solvation pressure is proportional to the volumetric strain, with adsorption stress defined as⁵³

$$P_{\rm s,sph} = -\frac{1}{4\pi R^2} \left(\frac{\partial \Omega_{\rm p}}{\partial R}\right)_{\mu,T},\tag{6}$$

where Ω_p is a grand thermodynamic potential of system in a single pore, and R is a pore radius. The GTP was determined via the NLDFT approach based on Rosenfeld's fundamental measure theory with the mean-field treatment of dispersion interactions. The derivative of GTP was performed numerically. The model was tested on the Xe and Kr adsorption on CaNaX zeolite and it demonstrated a good agreement with experimental data. The zeolite has a uniform 3D structure consisting of cavities ($\approx 1.2 \, \mathrm{nm}$) interconnected via windows.

The authors⁵³ used approximation of spherical pore with 0.75 nm radius, neglecting the connectivity effects. In addition, the effective density of oxygen atoms was adjusted in order to reproduce the pore-filling step on the experimental isotherms⁶¹. It is worth noting that the experimental adsorption-induced strain isotherms exhibit a minimum at a certain relative pressure. The model was capable to reproduce this non-monotonic behavior.

Recently, adsorption-induced deformation in materials with spherical pores was described using the DBdB theory, similar to Ref.49, and compared to the results of grand canonical Monte Carlo (GCMC) simulations⁶². The authors obtained the following expression for the adsorption stress in the fully filled pores⁶²:

$$P_{\rm s,full} = \frac{2\Delta\gamma}{R} + \frac{R_g T}{v_{\rm m}} \ln(p/p_0), \tag{7}$$

where $\Delta \gamma = \gamma_{\rm sl}$, i.e. the difference between the dry solid surface tension (stress) and surface tension on liquid-solid interface, $R_{\rm g}$ is the gas constant, and $v_{\rm m}$ is the bulk liquid molar volume. Here we also subtract the initial stress arising in the body due to the existence of surface stress of a dry surface^{63,64}. It is done to emphasize the fact that at small deformations it should not contribute to AID, which is primarily defined by the solid-fluid interactions and by the fluid structure. As one can see, the difference $\Delta \gamma$ defines the magnitude of the adsorption stress at the point $p/p_0=1$. It was estimated from Frumkin-Derjaguin equation and from the GCMC simulations. The latter significantly increases the agreement between solvation pressures calculated by theory and Monte Carlo simulation after the capillary condensation. However, it also qualitatively changes the behavior of theoretically calculated solvation pressure during pore filling: from the steep decrease to the steep increase.

We can summarize that both microscopic (DFT) and macroscopic (DBdB) approaches produce reasonable estimations of the adsorption stress magnitude. However, if in the case of microporous materials, the model results can be validated by the comparison with the experimental data, then in the case of mesoporous materials, the lack of experimental data on materials with spherical pores does not allow it.

D. Models with no host response: non-convex pores

In Ref.65 we developed a model of adsorption-induced deformation of CMK-3 like material. The feature of this material is in its pore geometry. Unlike the discussed above

the slit, cylindrical and spherical pores, which are common for microporous carbons, SBA, and MCM materials, CMK-3 (obtained as inverse replica of SBA-15⁶⁶) consisting of aligned cylinders results in complex nonconvex pore volume. In the model the pore geometry was simplified to the system of rods arranged in the hexagonal tiling and connected by virtual springs, responding for the flexibility. Thus, the total elastic free energy of the system can be written as:

$$F_{el} = \frac{3}{2} M \rho_{\rm spr} L \kappa (h - h_0)^2, \tag{8}$$

where M is number of rods in the system, κ is the spring constant and $\rho_{\rm spr}$ is springs density per rod length L. Since the springs were the only source of flexibility, other possible mechanisms like intrinsic rod relaxation or contribution arising from rod microporosity were neglected. It was shown that adsorption stress is proportional to the derivative of the GTP with respect to the spring length⁶⁵:

$$P_{\rm s,cmk} = -\frac{\sqrt{3}}{3ML(D_{\rm s} + h_0)} \left(\frac{\partial \Omega}{\partial h}\right)_{\mu, \rm T},\tag{9}$$

where $D_{\rm s}$ is the diameter of the carbon rod; the derivative was taken numerically via simple two-point estimation.

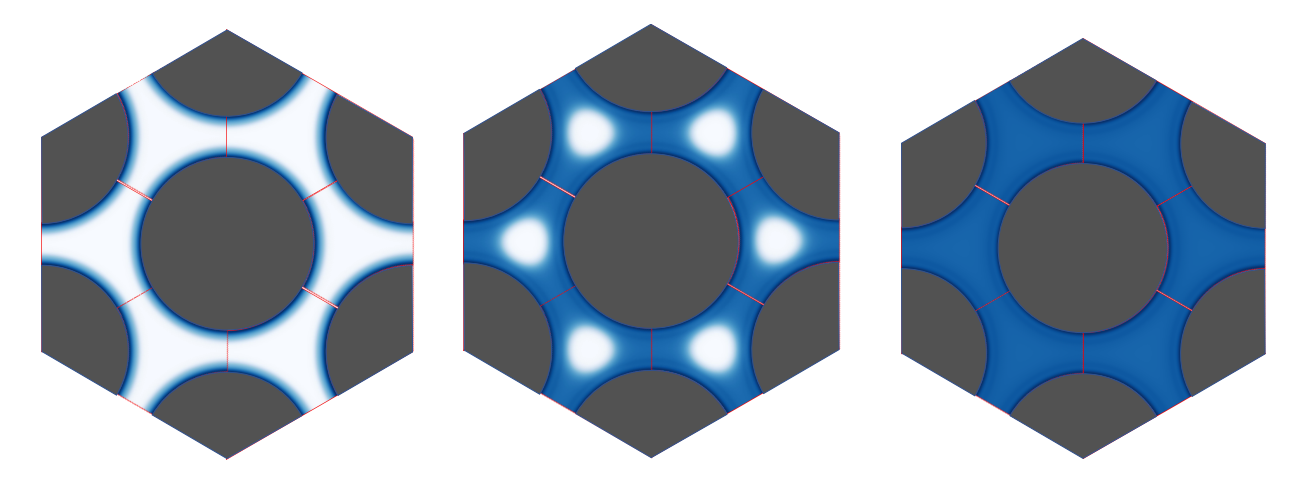


Figure 6: The three 2D density profiles during adsorption process in CMK-3 material at 77 K are shown. There are, from left to right, multilayer adsorption $(p/p_0 \simeq 0.3)$, bridging stage $(p/p_0 \simeq 0.43)$ and the filled pore $(p/p_0 \simeq 0.9)$. The gray circles represent carbon rods, the white color represents vapor phase, while the blue color — dense fluid phase.

Data is taken from Ref. 65.

Grand thermodynamic potential was calculated within the classical DFT framework,

namely van der Waals DFT⁶⁷. This version of DFT is based on the local density approximation applied for the description of short-range repulsive interactions and the mean-field treatment of attractive part of the intermolecular attractive potential. We choose the simplified version of DFT due to complexity of the problem — it does not reduce to one-dimensional, so that the Euler-Lagrange equation have to be solved on a two-dimensional grid. The latter leads to the significant increase of computational cost. The whole interparticle potential was taken as a square well potential with parameters fitted to nitrogen coexistence densities, vapor pressure, and surface tension at 77 K. The excess Helmholtz free energy was written as a sum of two contributions: Helmholtz free energy of the hard-sphere system and contribution of dispersion interactions. The first one is taken from the original formulation of FMT^{68} in homogeneous density limit and corresponds to the result of scaled-particle theory⁶⁹. The second one was estimated on the mean-field level. The external potential was taken as a superposition of seven one-rod potentials, where individual contribution was taken from Ref. 70. The model demonstrates three different adsorption stages, namely multilayer adsorption, bridge formation, and filled phase. The examples of density profiles corresponding to each of the stages are shown in Fig. 6 and the adsorption isotherms at three different temperatures are shown in Fig. 7. The temperature increase not only shifts the hysteresis to higher relative pressures, but also changes the shape of the hysteresis loop. One broad loop at 77 K first turns into two independent loops at 90 K and then, at 110 K, only one hysteresis remains. In addition, at the highest temperature, the bridge formation becomes reversible, while the remaining pore volume fills in the first order phase transition regime. Also, it was shown that the isotherms are sensitive to the distance between the rods, namely increase in intercylinder distance leads to a much broader hysteresis and an expectable absence on liquid bridges between them.

The adsorption stress isotherms plotted on Fig. 8 are different from slit, cylindrical and spherical ones. The stress in multilayer regime is almost negligible and then decreases during bridge progressive development. The first order phase transition during the bridge formation and capillary condensation turn into abrupt decrease of the solvation pressure at 77 K, on the other side, the reversible bridge formation at 110 K turns into continuous transition. It is worth noting that similar absence of solvation pressure during multilayer adsorption was observed in computer simulations⁷¹, where the authors studied the deformation in slit pore ($\approx 4 \, \text{nm}$ width) geometry. They have demonstrated that the normal to the pore walls

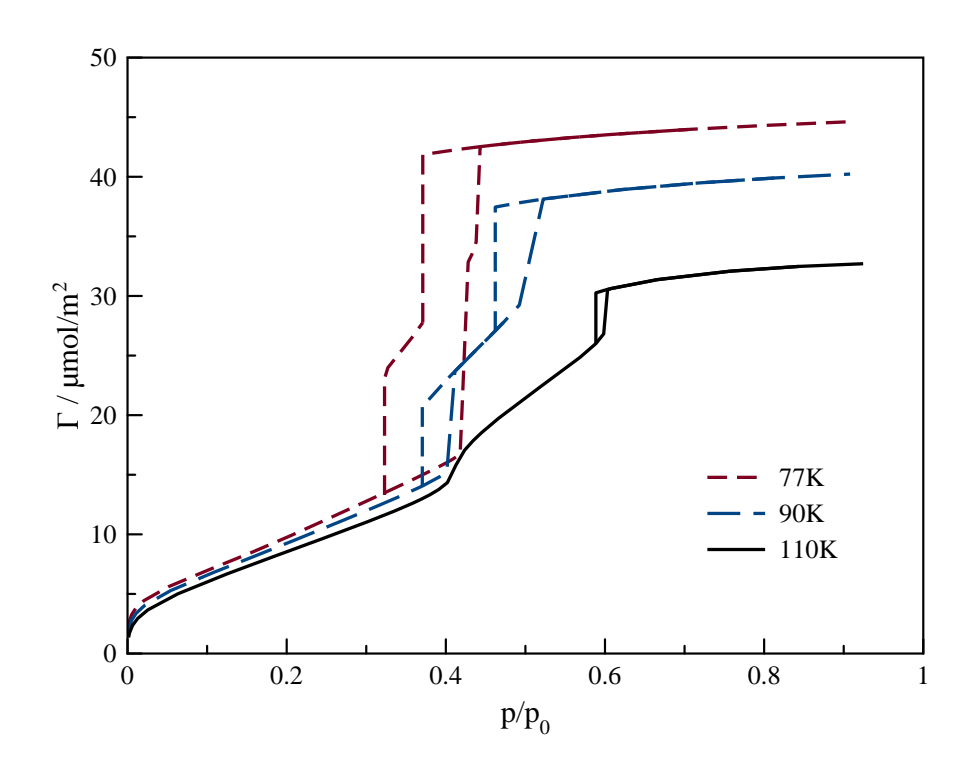


Figure 7: Calculated adsorption isotherms of CMK-3 material at 77 K, 90 K and 110 K. The model demonstrates three different adsorption stages, namely multilayer adsorption, bridge formation, and filled phase. The bridge formation is an intermediate stage on both adsorption and desorption branches of hysteresis. It manifests itself as a sudden change of adsorbed amount at 77 K and 90 K. At 110 K its formation takes place in a reversible fashion at $p/p_0 \approx 0.4$. An adsorption branch corresponds to the right branch of a hysteresis loop at the fixed temperature. Adsorption branches were calculated the following way: calculations were performed from the lowest relative pressure up to the highest, using the previously obtained density profile as a starting guess for the current point. Thus, the adsorption branch is generated as a metastable solution in the hysteresis region. On the other hand, desorption branches represent the true equilibrium solution of the present model. They were obtained by the comparison between the GTP of three different stages. Data is taken from Ref. 65.

deformation is negligible during multilayer adsorption and the strain in the filled pore mainly originates from Laplace pressure. So, both these works^{65,71} demonstrate the absence of the Bangham's like expansion in the direction normal to the pore walls.

Recently, the adsorption-induced deformation of hierarchical carbon materials with non-

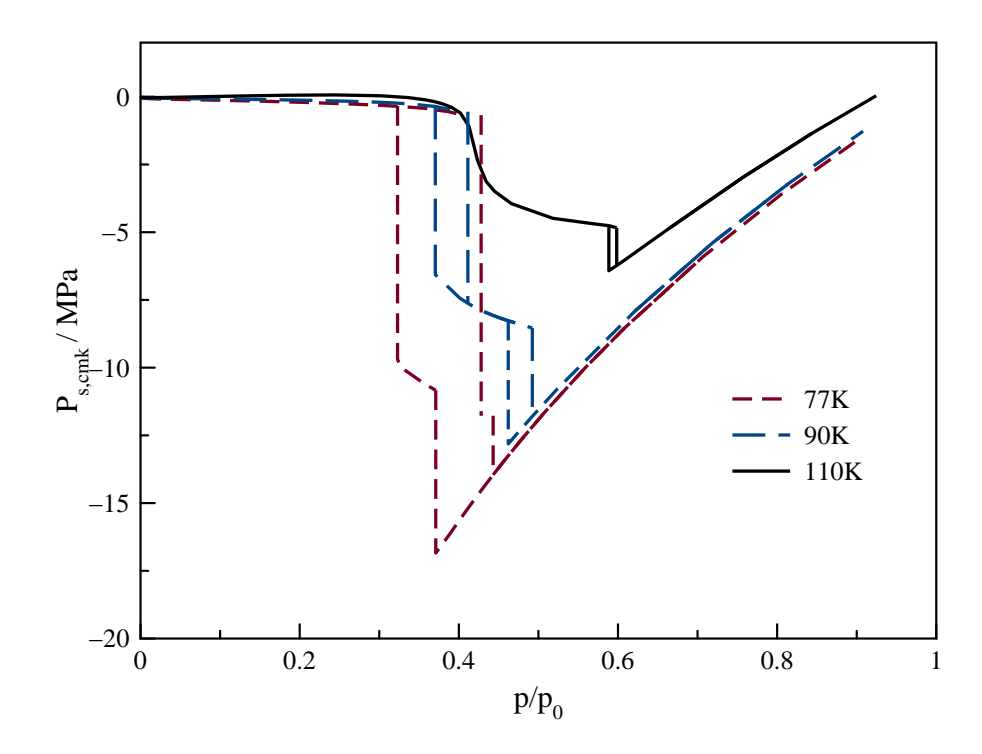


Figure 8: Calculated adsorption stress isotherms of CMK-3 material at 77 K, 90 K, and 110 K. An adsorption branch corresponds to the right branch of a hysteresis loop at the fixed temperature. The sharp vertical lines denote the positions of phase transitions in the system, the magnitude of the stress change on adsorption branches were only estimated. The more rigorous calculations were problematic due to the discontinuous nature of the phase transition. Data is taken from Ref. 65.

convex pores were measured by means of small-angle neutron scattering (SANS) and dilatometry⁷². The experimental results are qualitatively different from those obtained for convex pore geometries and suggest the existence of three relative pressure intervals with distinct strain behavior. Although the SANS results confirm the general contraction behavior predicted by the model, the detailed comparison shows some deviations. Namely, the contraction at low relative pressure and increase of adsorption stress along the hypothetical bridge phase development. It should be noted, that experiments were performed with n-pentane at 290.15 K, while the calculations were made for nitrogen at 77 K. Besides this obvious difference, the local nature of the DFT and the idealized picture of the adsorbent (virtual interconnections and ideal carbon rods packing) could be a reason for the discrepancies.

E. Models with linear host response

Up to now, we have described only models in which the coupling between adsorption and deformation processes was disregarded. It is correct only for a sufficiently stiff porous materials and thus the applicability of these models depends on it. In Ref.73 the authors observed the difference between two adsorption isotherms measured on free-standing and attached to the underlying silicon wafer porous membranes, and attributed it to a mechanical effects. In particular, this result has increased an interest in studying the effect of AID on adsorption process. Recently, Bossert et al.⁷⁴ measured adsorption isotherms of porous silicon submitted to an external stress or strain. Applying the strain ($\approx 10^{-3}$) the authors did not obtain any measurable changes in the adsorbed amount. The latter should also be try for a solid with similar elastic modulus and magnitude of deformation. In addition, the authors⁷⁴ suggest that the results obtained in Ref.73 could be due to the small differences between the geometry of the samples. However, the adsorption-deformation coupling is still important for softer materials (e.g. aerogels and polymers) and its account reveal the difference in adsorption process on rigid and flexible solids.

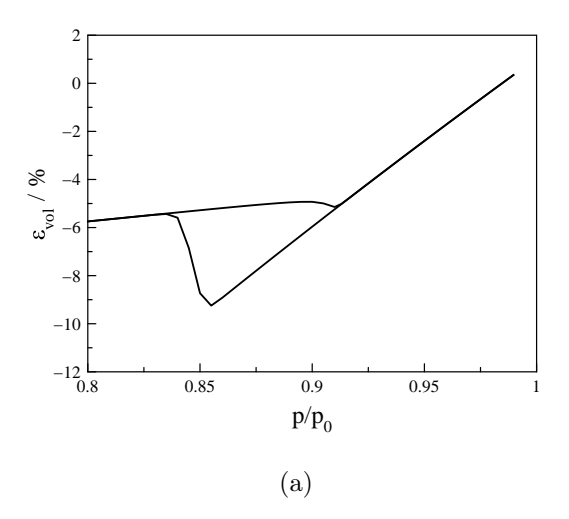
In the Ref.35 Ustinov and Do extended a model of adsorption-induced deformation in a slit pore. The GTP was calculated within the DFT in Curtin-Ashcroft-Tarazona weighted density approximation^{41,75}; the elastic free energy is written in the Hooke's approximation (the two pore walls are connected via a virtual spring) with initial pressure at zero loading due to the wall-wall interactions. The pore wall was modeled as a set of carbon layers and the numerical calculations were performed for nitrogen at 77 K. Minimizing Eq.(1) with respect to two order parameters — pore width and density profile, the authors obtained the system of two coupled equations, defining the adsorbate density profile and corresponding pore size. Thus, the authors took into account the coupling between adsorption and deformation processes. The following expression for the solvation pressure was introduced³⁵:

$$f = \Pi_s(H) - \int_{-H/2}^{H/2} \rho(z)\phi'_{\rm sf}(H/2 - z)dz - \Pi_0 - P, \tag{10}$$

where the first term is the contribution due to the solid-solid interactions in the equilibrium configuration, the second term is the contribution arising from the adsorbent (which defines the AID), the third term is the initial stress and $\phi'_{\rm sf}(H/2-z)$ is a derivative of the solid-fluid potential of interactions. Now, the equation of mechanical equilibrium takes the simple form

 $f = E(H - H_0)/H_0$, where E is a Young's modulus of an imaginary spring connecting the walls. The authors investigated the effect of pore softness on adsorption process, comparing the results in flexible and rigid pores. The strain produce the most significant effect in the smallest pores ($<1\,\mathrm{nm}$) and becomes insignificant if their width becomes greater than 1.3 nm (the calculations were preformed with $E = 5\,\mathrm{GPa}$). In general, the deformation resulted in the shift of the pore filling toward smaller relative pressures. However, in some pores (for instance 0.8 nm and 0.9 nm) it also changes the pore filling mechanism from continuous in rigid pores to a first-order transition in flexible pores. It was also demonstrated, that the fluid distribution can be significantly affected by the pore deformation. In the rigid pore of 0.83 nm width the density profile represents a two-layer structure, but in a sufficient soft pore ($E < 5\,\mathrm{GPa}$) the fluid is rearranged to a single layer structure centered in the middle of the pore. The latter happens due to the contractive nature of the solvation pressure at this particular pore size. The authors showed that the adsorption-deformation coupling can also affect the other fluid-solid thermodynamic properties, such as the heat of adsorption³⁵.

In general, adsorption stress reduces with an increase of a pore size, which makes it more pronounced in micropores (see, for instance Fig.3). However, it does not mean that AID should be always neglected during the study of adsorption on mesoporous materials. It is clear that even relatively small solvation pressure will result in a significant deformation if the elastic constant of the solid body is small. Perhaps one of the most obvious examples of such materials is aerogels. Having extremely high porosity, they demonstrate pronounced AID and manifest adsorption-deformation coupling^{8,9}. In Ref. 36, Kolesnikov et al. presented a model of adsorption-induced deformation of mesoporous materials, basing on the minimization of the thermodynamic potential Eq.(2). The adsorption part of the model inherits the assumptions of the well-known DBdB model, while the deformation part utilities Hooke's law and the assumption of solid incompressibility. In the limit of rigid material the results reduces to ones from the DBdB theory. The minimization procedure, similar to the one in the previously described theory, produces the system of two coupled equation. They describe the joint evolution of strain and adsorption isotherms as the functions of relative pressure. Among other things, the authors discussed the deformation of a hypothetical soft material (see Fig.9). The Fig. 9a demonstrates the volumetric strain ($\epsilon_{\rm vol}$) isotherm, which is similar to one obtained for aerogel in experiments⁸ at high relative pressures. The adsorption isotherms corresponding to rigid and flexible mesoporous adsorbent are also presented



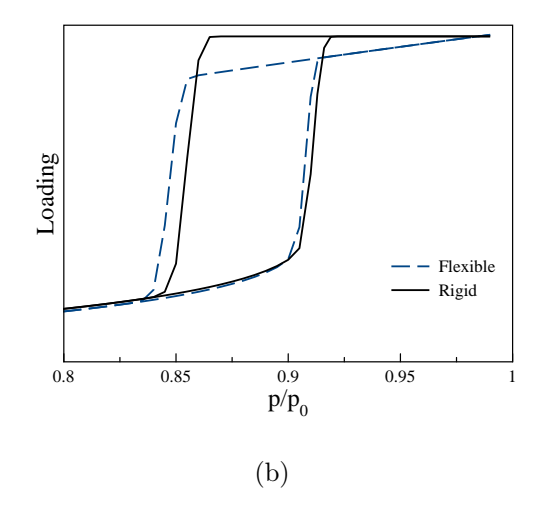


Figure 9: (a) The volumetric strain isotherm of the hypothetical flexible mesoporous adsorbent with pore load modulus equal to 20 MPa. (b) Theoretical adsorption isotherms corresponding to rigid and flexible (pore load modulus is 20 MPa) hypothetical mesoporous adsorbent. Data is taken from Ref. 36

in Fig. 9b. The Gaussian PSD with an average pore width 16 nm was used for "smoothing" of both isotherms. The isotherm of a rigid material reproduces the H1 hysteresis type (see Fig.9 and the caption), while the isotherm of flexible material demonstrates some deviations. Namely, the hysteresis branches are shifted to lower relative pressures and the saturation plateau is now replaced with a monotonic increase. Both deviations are due to the change of the pore size, which reaches its lowest value right before the inset of evaporation. If now one will apply the standard characterization methods (Kelvin equation, BJH, NLDFT, etc.) to the "flexible" isotherm it will give an erroneous pore-size distribution. Thus, strain isotherms not only provide a useful additional (to standard adsorption isotherms) information, but also could be vital for the understanding and characterization of a soft porous material.

F. Models with non-linear host response

In contrast to the materials which undergo only elastic deformations, MOFs can undergo both elastic deformations and structural transformations. The latter can be treated as transitions between different phases of the solid framework (for example "gate-opening" and "breathing"). The theoretical description of these systems is also complicated by the

fact that the elastic properties can be highly anisotropic⁷⁶. However, even in this case, the simple thermodynamic models could provide reasonable insights into the adsorption-induced deformation. Below we discuss the models which on the one hand are based on the same ideas as those applied for the description of linear elastic materials, but on the other hand, highlight the importance of coupling between adsorption and deformation.

In Ref.19 Coudert et al. developed a thermodynamic description of adsorption into a flexible framework, which can undergo an adsorption-induced structural transition. The description is based on the comparison between the thermodynamic potentials (see Eq.(1)) of different structures. The corresponding grand thermodynamic potentials are determined by the integration of the standard thermodynamic equation (2). The elastic deformations within each of the phases was disregarded. Thus, Ω can be obtained from a bunch of classical adsorption isotherms and even estimated from an experimental data. As adsorbed amount (N) corresponds to a hypothetical adsorption isotherm of a certain rigid solid phase of a host material, only a part of it can be measured experimentally. Evidently, the measurement of an entire isotherm requires a material which is identical to the one investigated, but does not undergo a structural transition. The proposed method allows estimating the number of structural transitions, their positions, i.e. relative pressures, and a difference between Helmholtz free energy of two "coexisting" solid phases. However, the approach is applicable only to the true equilibrium path and cannot describe hysteresis on MOF adsorption isotherms, which is commonly observed in numerous experiments.

Another model was proposed by Neimark et al.⁷⁷, shifting the focus from pure thermodynamic description to a mechanistic one. The authors supposed that structural transition of MOFs occurs when adsorption-induced stress reaches a certain value. The particular focus was on xenon adsorption on MIL-53(Al) at 220 K⁷⁸, which demonstrated a pronounced breathing with two hysteresis loops. The grand thermodynamic potential was defined via Eq.(2) for each crystal phase lp and np applying Langmuir isotherm equation for both of them independently. The adsorption-induced stress was calculated as a derivative of the GTP of an adsorbed phase per unit cell with respect to the cell volume at the fixed temperature and chemical potential⁷⁷:

$$P_s(p,T) = R_{\rm g} T \left\{ \frac{\mathrm{d}N_0}{\mathrm{d}V_{\rm c}} \left[\ln(1 + K_{\rm H} p/N_0) - \frac{K_{\rm H} p/N_0}{1 + K_{\rm H} p/N_0} \right] + \frac{\mathrm{d}K_{\rm H}}{\mathrm{d}V_{\rm c}} \left(\frac{p}{1 + k_{\rm H} p/N_0} \right) \right\}, \quad (11)$$

where N_0 is the unit cell capacity, $K_{\rm H}$ is the Henry's constant and $R_{\rm g}$ is the gas constant.

The unknown derivatives dN_0/dV_c and dK_H/dV_c as well as the critical stresses, at which the structural transition happens, were adjusted to the experimental data. It appears that $dN_0/dV_c > 0$ and $dK_H/dV_c < 0$, this difference in sign leads to a non-monotonic behavior of adsorption-induced stress and, thus, allows one to describe the position of both hysteresis remarkably well. In the Henry region $P_s(p,T) \approx R_g T p dK_H/dV_c$, and thus the initial contraction is possible only if the affinity constant is a decreasing function of the pore volume.

Watanabe et al.⁷⁹, by means of GCMC simulations, performed the analysis of the grand thermodynamic potential profile of a flexible framework during fluid adsorption. The profile was calculated as a continuous function of the reaction coordinate via the method of thermodynamic integration. The authors demonstrated that a gate-opening is accompanied by the formation of an additional minimum on the energy profile, which is stabilized by the adsorbate presence. In addition, it was proposed that the observed energy barrier could be the origin of the hysteresis on the adsorption isotherm. This idea was further examined by Bousquet et al.¹⁸ in the theoretical approach based on the osmotic ensemble. In this particular case Eq. (1) was written as follows¹⁸

$$\Delta G(\alpha, p, T) = F_{\text{host}}(\alpha, T) - R_{\text{g}}T \int_{0}^{p} \frac{K_{\text{H}}(\alpha, T)p}{1 + K_{\text{H}}(\alpha, T)/N_{\text{max}}(\alpha, T)} V_{\text{m}}(p, T) dp + pV_{\text{host}}(\alpha), \quad (12)$$

where $V_{\rm m}(p,T)=(\partial\mu/\partial p)_{\rm T}$ is a molar volume of the bulk fluid, and one can recognize the Langmuir equation in the integrand. In contrast to the previous works, the authors introduced an order parameter - α (for instance, one of the angles in a pore), which describes the evolution of the flexible framework. The positions and depths of the minima on the $\Delta G(\alpha,p,T)$ define the adsorption behavior in the flexible solid. Thus, the particular profile of the osmotic potential is mainly defined by the dependencies of the Henry's constant, saturation uptake amount and free energy of host material on an order parameter α . Basing on the general considerations and the results of GCMC simulations the authors suggested the ad hoc analytical functions for both $N_{\rm max}(\alpha,T)$ and $K_{\rm H}(\alpha,T)$. The resulting Henry's constant has a pronounced maximum and this point was called single point most comfortable structure ($\alpha_{\rm MCS}$), i.e. the point where a fluid molecule nicely fits into the pore and interact with multiple pore walls. The authors considered monostable and multistable Helmholtz host free energies, i.e. the case when $F_{\rm host}(\alpha,T)$ has one or more than one minimum, respectively.

The authors demonstrated that the ratio $\alpha_{\rm MCS}/\alpha_0$ (where α_0 is the minimum of the monostable host free energy) defines the evolution of the order parameter. If $\alpha_0 > \alpha_{\rm MCS}$

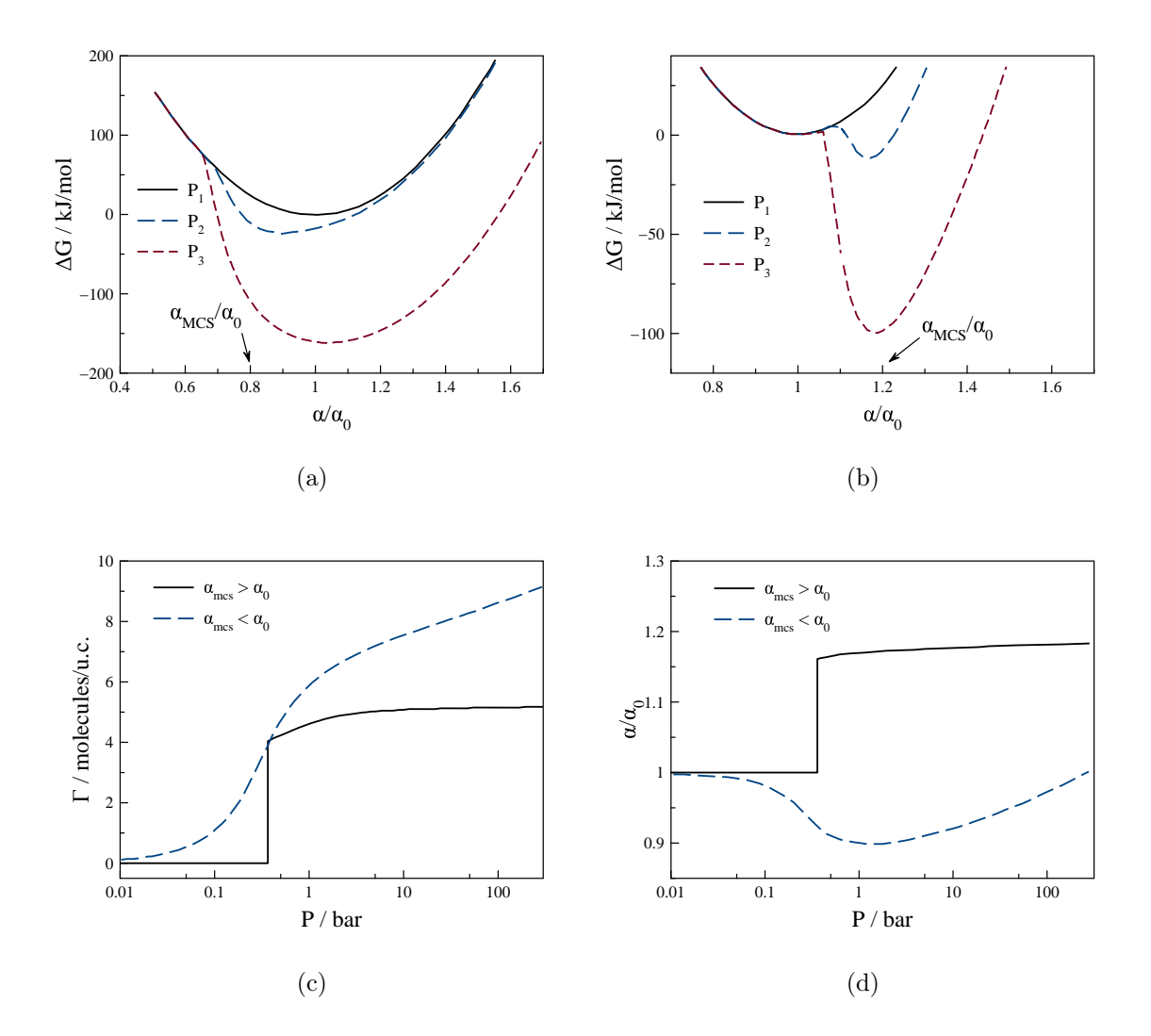


Figure 10: (a,b) Solvation Gibbs free energy as a function of the pore opening angle α at three different adsorbate pressures $(P_1 < P_2 < P_3)$ for $\alpha_{\text{MCS}} < \alpha_0$ and $\alpha_{\text{MCS}} > \alpha_0$, respectively. (c) Adsorbed amount per unit cell as a function of the adsorbate pressure. (d) Pore opening angle as a function of the adsorbate pressure. The pore evolution remarkably depends on the ratio $\alpha_{\text{MCS}}/\alpha_0$ and demonstrates the fist-order like structural transition in one of the cases $(\alpha_{\text{MCS}} > \alpha_0)$. Data is taken form Ref.18.

AID is a continuous non-monotonic process with a minimum at low pressure values, which is typical for a number of microporous adsorbents. On the other hand, if $\alpha_0 < \alpha_{\text{MCS}}$ adsorption-induced deformation takes place as a first-order transition (see. Fig.10), which is resembles the adsorption-induced "gate-opening". It is also similar to the change of the pore filling mechanism obtained for a flexible slit pore³⁵ which was discussed in the previous section.

Usage of a bistable host free energy leads to a greater variety of possible scenarios, that include "breathing" among others.

Of course, there are many more models aiming to describe metal-organic frameworks behavior both adsorption-induced^{80–83} and induced by other stimuli^{56,78}. However, their comprehensive description is clearly beyond the scope of the present review. The discussed works demonstrate the importance of the account of adsorption-deformation coupling in the description of the metal-organic framework.

III. EFFECT OF A PORE SIZE DISTRIBUTION ON ADSORPTION-INDUCED DEFORMATION

Up to now, we discussed adsorbents as a solid material with a unimodal pore size distribution, which is an approximation (for some ordered materials indeed a good one). However, the question of how a certain PSD will affect the adsorption-induced deformation is of course important. Its answer will not only give us a better understanding of the AID phenomenon but can also open new possibilities for material characterization. In this section, we would like to discuss the main effects and problems that arise due to an account for a pore size distribution (PSD) in the AID models.

The role of the pore size distribution in the description of solvation pressure in slit-like pores were studied for the first time in the work²⁹ by Frink and van Swol. By means of classical density functional theory based on Rosenfeld's FMT and mean-field treatment of dispersion interactions, the authors calculated the adsorption stress for a set of pores by Eq.(3) and estimated PSD effect as²⁹:

$$\langle P_{\text{s,slit}} \rangle (p) = \int_{0}^{\infty} dH P_{\text{s,slit}}(H, p) g(H),$$
 (13)

i.e. average of an ensemble of pores; g(H) defines the probability of presence of the pore with size H. From this equation, one can see that the PSD will result in the smoothing of the stress at a fixed bulk pressure. The authors explored the possibility to extract different adsorption-related properties from solvation pressure isotherms. In the case of bimodal distributions, where one mode is in the mesoporous region, it was suggested that the size of the mesopores can be approximated from the position of the dip on the isotherm (which is correspond to the hysteresis region). It was shown that the averaged adsorption stress at

saturation in microporous range is sensitive to the width of the distribution, which can be also used for the PSD determination. In addition, the authors demonstrated that the onset of adsorption stress is more sensitive to the energetic parameter of solid-fluid interaction than to the width or average pore size.

In the work⁸⁴, Kowalczyk et al. presented the model of adsorption-induced deformation of microporous carbon. The sample strain is assumed to arise from the pores volume change only, i.e. the solid only transfers the deformation but is incompressible itself. The adsorption stress is defined in a standard for slit pores way — through Eq.(3), and was calculated via Monte Carlo simulations. The flexibility of each pore was described by a presence of a virtual spring with a certain stiffness constant — k. The typical activated carbon has a pore size distribution, and the authors demonstrated that its effect can be taken into account⁸⁴:

$$\epsilon_{\text{vol}}(p) = \frac{1}{M} \left(\frac{\int dH P_{\text{s,slit}}(H, p) S(H) H}{\int dH S(H) H} - p \right), \tag{14}$$

where $\epsilon_{\text{vol}}(p)$ is the volumetric strain, and $\frac{1}{2}HS(H)dH$ is the volume of pores of width from the interval (H, H + dH). Thus, the volumetric AID in the solid with a certain PSD is defined by the adsorption stress averaged by the pore volume distribution. Also, an effective bulk modulus was introduced as $M = k/\phi$, where ϕ is the sample porosity. The model was tested on the argon adsorption at 243 K. The authors showed that the different pore size distributions lead to qualitatively different strain isotherms, including the nonmonotonic one. The reason for this behavior lies in the oscillatory nature of solvation pressure with respect to the pore size variation (see, Fig.2).

Interestingly the similar equation was derived in Ref.85 based on the different assumptions: homogeneous and isotropic volumetric deformation of the entire porous solid is coupled to a certain law of pore radius change $R_i(\epsilon) = R_i^0(1 + \epsilon_{\text{vol}}/3)$ (where $R_i(\epsilon_{\text{vol}})$ and R_i^0 is an actual and reference size of the *i*-th pore respectively). The latter means that all pores will deform in a similar fashion at a fixed value of ϵ_{vol} , thus the authors neglected the local heterogeneity of the pore deformation. With a few examples the authors demonstrated the influence of PSD on the strain isotherms of mesoporous materials. Namely, it smooths the abrupt condensation/evaporation transitions similarly to adsorption isotherms (see Fig.(11b)), which allows one to describe experimental data^{36,85} better. The similar idea of strain pore size coupling was recently applied in the study of sorption hysteresis in nanoporous polymers⁸⁶. The authors used the idea that pores exposed to AID affect their

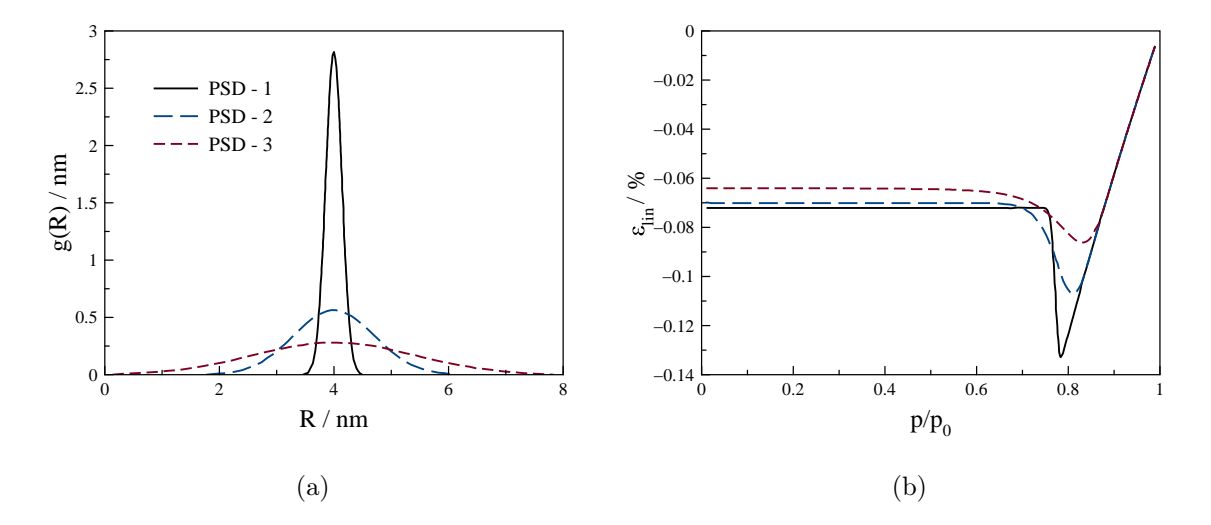


Figure 11: (a) Three Gaussian-like different pore size distributions centered around 4 nm pore. (b) The relative length change (ϵ_{lin}) as a function of relative pressure for all three PSD. The calculations were performed in the framework of classical theory of capillarity applied for the cylindrical geometry. The legend from the left figure correspond to the right one as well. Data is taken from Ref.85.

neighbors. For example, if a pore, adsorbs some amount of fluid and swell then the pores connected to it will experience adsorption-induced strain as well. Moreover, it happens even if they are not broad enough to adsorb on their own. Thus, if there are some amount of pores which are not able to adsorb a certain fluid due to steric reason then they can be "opened" by their neighbors during the sample filling. The adsorption process into pores was described via the Langmuir-like equation, while the coupling between adsorption and deformation was taken into account by means of poromechanics. The authors demonstrated that the model is in agreement with the results of molecular simulations of water adsorption into amorphous cellulose⁸⁷.

Since a strain isotherm contains information about the pore size distribution of a material, one can look at it from a different angle and recover the distribution⁵¹. It is not a trivial problem, because the adsorption-induced strain may be affected by numerous factors, like pore geometry and their interconnections, the spatial distribution of pores with different widths in the material, chemical heterogeneities on the pore walls, etc. However, in some cases, the above described averaging of solvation stress (or similar ones) provides good

results. In particular, it was demonstrated³⁶ on water adsorption on Vycor glass² – the peak and the width of the PSD obtained from adsorption and deformation data are in good agreement. Another worth mentioning works^{27,28} are focused on the microporous carbons. The authors showed that the strain isotherms can be used as a complementary approach to investigate the porous structure and even complement the classical methods basing on adsorption isotherm analysis. The latter is of particular importance, because most of the adsorbent properties are usually determined indirectly, relying on a quality of theoretical models. Thus, accounting for AID within existing theoretical frameworks (e.g. DBdB and DFT) leads to their critical assessment and further improvements in characterization methodology of porous solids.

IV. MODELS OF DISORDERED MATERIALS

Consideration of materials in which pores do not have a well-defined geometry is necessary for developing theories of adsorption and adsorption-induced deformation. Such theories would allow to study the effects of local heterogeneities and to predict the AID of realistic materials. We note that the account of a PSD as it was described in the previous section - Eq.(13), is generally valid for material with independent pores. On the other hand, disordered materials demonstrate blocking and cavitation effects altering the hysteresis type, i.e. transitioning from H1 to H2⁸⁸. It is accompanied by the change of the hysteresis width and slope and can provide valuable information about the interconnection of the pore network. Simultaneously, it restricts the theoretical methods which can be used for its prediction/description – due to the complex pore connectivity one needs to consider a larger sample volume. One of the frequently used methods is the mean-field lattice density functional theory (lattice MFDFT)^{89,90}. For instance, it was recently used to study nitrogen adsorption in three-dimensional geometrical models of silica⁹¹ obtained by electron tomography. Fig. 12 shows a comparison between two hysteresis loops (nitrogen at 77 K, SBA-15) one calculated with the lattice MFDFT and the experimental one. The theoretical results demonstrate a good agreement with the experiment, in particular narrow hysteresis loop with parallel and steep branches. However, the model significantly underestimates adsorbed amount at lower relative pressures. Thus, one can conclude that an on-lattice model is a good approach to describe adsorption process in a realistic pore network. Its applicability to the description of AID will be discussed below in the present section.

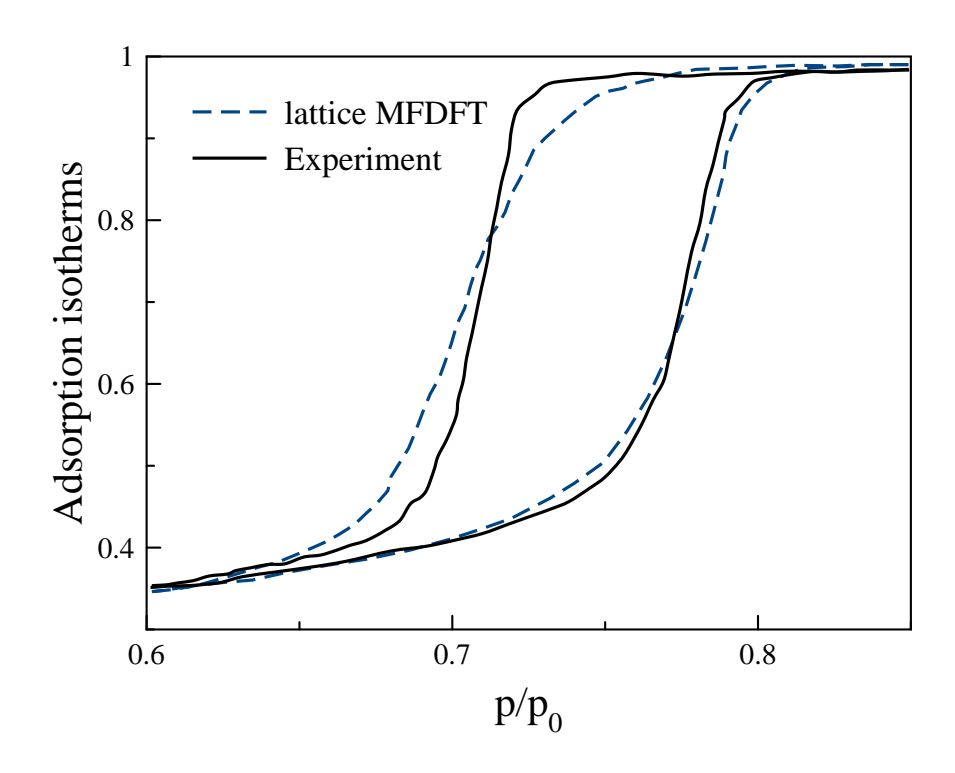


Figure 12: Nitrogen adsorption isotherms at 77 K: experimental data for an SBA-15 silica sample, and theoretical predictions using the lattice MFDFT framework. Data is taken from Ref.91.

In principle, the Bangham's law^{92–94} and its revision⁹⁵, based on the surface stress formalism, can be attributed to this section — both of them do not depend on the pore volume definition (both of these methods and other classical ones were recently reviewed¹, so we will not dwell on them). Recently, El Tabbal et al.⁹⁶ presented a poromechanical model for drying of unsaturated material. The authors focused on the study of water in meso-and macropores. The model takes into account the capillary, adsorption (or Bangham), and Shuttleworth effects, where the latter considers the variation of surface energy with respect to the skeleton strain. The model was validated on a set of experimental data^{2,97,98}, demonstrating promising results.

Some models employing the usage of Eq.(2) also belong here. Using different adsorption isotherms, one will obtain a corresponding adsorption stress differentiating the obtained GTP by volume at fixed temperature and pressure (see. Eq.(11) for example). Lately, this approach was used in combination with potential adsorption theory⁹⁹ (in the particular case

of Dubinin-Radushkevich equation¹⁰⁰) and applied to the description of AID of microporous carbon under benzene and n-hexane adsorption. Despite the success of these macroscopic models the lack of microscopic details imposes some limitations.

In Ref.101 Guyer and Kim developed a theoretical framework which can be applied to bodies with different pore geometries with equal success. The theory is based on finite element method and was made for 2D system. Fluid and solid free energy are based on the mean-field lattice DFT⁸⁹ and the linear elasticity theory, respectively. The key point of the approach is the introduction of the additional parameter describing the solid-fluid elastic coupling. The total coupling term is a sum of two contributions¹⁰¹:

$$F_{\rm sf} = \frac{1}{2} \sum_{i} \rho_{\rm i} \left(U_{\rm i} + W_{\rm i} (\nabla \cdot \mathbf{u})_{\rm i} \right), \tag{15}$$

where the first one is a wetting term and the second one is the elastic free energy accounting for the fluid presence. The notations are: U_i are the parameters of solid-fluid energy of interactions, $\rho_{\rm i}$ is the fluid density in element i, $W_{\rm i}$ are the parameters of elastic coupling, $(\nabla \cdot \mathbf{u})_i$ is the strain at *i*-th element, and the summation is performed over all elements in the system. The authors demonstrated, that the coupling between the strain and fluid density results in the hysteresis behavior, and called it emergent hysteresis. This behavior is similar to the presence of the phase transition in flexible slit pores (Ustinov and Do³⁵) and to the step-wise isotherms of flexible MOFs. A similar approach was used by Bakhshian et~al. for the description of fluid adsorption into the sandstone and the accompanying deformation of the solid. The authors used the same coupling term, i.e. Eq. (15), but the whole framework was extended to the 3D case. In addition, a real sandstone structure was used in order to produce a representative model of solid phase. The model was capable to describe adsorption and strain isotherms of CO₂ and N₂ with good accuracy, by means of only one fitting parameter – $W_i = const$, i.e. independent on the lattice position. It should be mentioned, that the density defining the chemical potential of the bulk fluid in lattice-gas approximation was obtained from the Peng-Robinson equation of state. It, apparently, leads to a better agreement with experimental data. However, it also introduces inconsistency into the model, because the Peng-Robinson equation of state and the one obtained for the meanfield lattice gas do not match.

Another lattice-based approach was proposed in the work Zhou $et\ al.^{103}$ in which adsorption and moisture-induced capillary stress was studied. The authors developed a complex

three-stage procedure to obtain the induced deformation of a mesoscale model nanogranular cement¹⁰⁴. The lattice size, fluid-fluid interaction parameter and fluid-solid interaction parameter were estimated from the surface tension, bulk critical temperature and water isosteric heat of adsorption at zero coverage in the cement paste. The authors started from the calculation of the adsorption/desorption isotherms by means of lattice density functional theory⁸⁹, simultaneously obtaining the fluid distribution corresponding to each value of the adsorbed amount. In its turn, the capillary stress due to the fluid distribution was calculated based on the capillary stress tensor^{105,106}. In order to predict the cement mechanical response, the authors used the modified molecular dynamics simulation, where the resulting adsorption-induced forces were additionally applied to the nanograins. The obtained results are in a very good agreement with experimental results^{107,108} on both "aged" and "hardened" cement sample. Despite the success, the general applicability of the method is unclear because it is based on the lattice-gas EOS without any specificity inherent in water systems and requires additional MD usage.

Thus, the microscopic models are capable of predicting the adsorption and adsorption-induced deformation on the realistic disordered materials. However it requires not only a good description of bulk and confinement fluid (which could be a problem in the case of lattice-gas EOS), but also an additional method for the strain evaluation. On the other hand, the macroscopic models are good tool for a fast data evaluation on the sample scale level, if the disordered solid structure does not reveal itself.

V. CONCLUSION

In this review, we covered the recent theoretical results in the field of adsorption-induced deformation and showed the connection between them and previous works. Starting from the models of ordered materials, we discussed the effects of pore geometry, linear and non-linear adsorption-deformation coupling, pore size distribution on strain and adsorption isotherms. We summarized all the considered models with the main references in Table I.

The pore geometry affects the adsorption stress isotherms and while in the case of classical idealized pores (slit, cylindrical and spherical) its influence is typically minor, for non-idealized pores it can qualitatively change the predicted trends. The CMK-3 material is a perfect example – both model and experiment suggest significant deviations from the pre-

Model	Geometry	Reference
Ordered materials (no host response)	slit geometry	40, 45, 28
	cylindrical geometry	49, 55
	spherical geometry	53, 62
		65
Ordered materials (with linear host response)	slit geometry	35
	cylindrical geometry	36
Materials with non-linear host response		19, 77, 18
Effect of PSD	slit geometry	29, 84, 85, 28
	cylindrical geometry	36
Disordered materials		101, 102, 103

Table I: Comparative summary of models for adsorption-induced deformation with the selected references.

viously observed patterns. Their sources are still debatable and therefore require more detailed theoretical and experimental investigations. Partly this also applies to the pores with corrugated cylindrical and spherical geometries, for which there are models and computer simulations, but the lack of high resolution experimental data in the mesoporous range does not allow to validate them. However, the existing results suggest that deformation isotherms in some cases are more sensitive to the pore geometry, and thus can be utilized for porous materials characterization.

For several classes of porous materials, the adsorption process can be strongly affected by the presence of AID: aerogels, porous polymers, MOFs. Several models demonstrate the change of microporous filling mechanism in the flexible pores, namely the occurrence of hysteresis¹⁰¹ or first-order like pore filling^{18,35}, which in the case of MOFs is called gate-opening. In the mesoporous solids, the main effect is in the shift of adsorption isotherm hysteresis branches and the replacement of the plateau (after capillary condensation) with a progressive filling. Both deviations are due to the change of PSD in the material. Thus, taking into account AID is of importance for the PSD determination in soft materials, however, there is not enough experimental data to assess the area of applicability of the

existing models.

Despite the present success in the description of AID in disordered materials, it is still the challenging task. The models with realistic 3D solids require additional tools to deal with the elastic part of the problem and that can lead to a significant increase in complexity. Due to the solid detailed picture, the consistency requires the determination of 3D fluid density distribution. The latter depends on the quality of the inhomogeneous adsorbent model and the bulk equation of state. The use of lattice-gas-based theory allows us to obtain inhomogeneous fluid distribution on a sufficient scale, however inherits all the disadvantages of the lattice-gas EOS.

ACKNOWLEDGMENTS

Y.A.B. acknowledges support within the Project Teams framework of MIEM HSE. G.Y.G. acknowledges the support by the National Science Foundation under Grant No. CBET-1944495

REFERENCES

- ¹G. Y. Gor, P. Huber, and N. Bernstein, "Adsorption-induced deformation of nanoporous materials a review," Applied Physics Reviews 4, 011303 (2017).
- ²C. Amberg and R. McIntosh, "A study of adsorption hysteresis by means of length changes of a rod of porous glass," Canadian Journal of Chemistry **30**, 1012–1032 (1952).
- ³G. Y. Gor, O. Paris, J. Prass, P. A. Russo, M. M. L. Ribeiro Carrott, and A. V. Neimark, "Adsorption of n-pentane on mesoporous silica and adsorbent deformation," Langmuir **29**, 8601–8608 (2013).
- ⁴C. Boissiere, D. Grosso, S. Lepoutre, L. Nicole, A. B. Bruneau, and C. Sanchez, "Porosity and mechanical properties of mesoporous thin films assessed by environmental ellipsometric porosimetry," Langmuir **21**, 12362–12371 (2005).
- ⁵P. Sharifi, B. Marmiroli, B. Sartori, F. Cacho-Nerin, J. Keckes, H. Amenitsch, and O. Paris, "Humidity-driven deformation of ordered mesoporous silica films," Bioinspired, Biomimetic and Nanobiomaterials **3**, 183–190 (2014).

- ⁶A. Grosman, J. Puibasset, and E. Rolley, "Adsorption-induced strain of a nanoscale silicon honeycomb," EPL (Europhysics Letters) **109**, 56002 (2015).
- ⁷M. Champeau, J.-M. Thomassin, C. Jérôme, and T. Tassaing, "In situ FTIR microspectroscopy to investigate polymeric fibers under supercritical carbon dioxide: CO₂ sorption and swelling measurements," The Journal of Supercritical Fluids **90**, 44–52 (2014).
- ⁸G. Reichenauer and G. Scherer, "Nitrogen sorption in aerogels," Journal of non-crystalline solids **285**, 167–174 (2001).
- ⁹G. W. Scherer, D. M. Smith, and D. Stein, "Deformation of aerogels during characterization," Journal of non-crystalline solids **186**, 309–315 (1995).
- ¹⁰C. Serre, S. Bourrelly, A. Vimont, N. A. Ramsahye, G. Maurin, P. L. Llewellyn, M. Daturi, Y. Filinchuk, O. Leynaud, P. Barnes, et al., "An explanation for the very large breathing effect of a metal-organic framework during CO₂ adsorption," Advanced materials 19, 2246–2251 (2007).
- ¹¹Y. Liu, J.-H. Her, A. Dailly, A. J. Ramirez-Cuesta, D. A. Neumann, and C. M. Brown, "Reversible structural transition in MIL-53 with large temperature hysteresis," Journal of the American Chemical Society **130**, 11813–11818 (2008).
- ¹²I. Beurroies, M. Boulhout, P. L. Llewellyn, B. Kuchta, G. Férey, C. Serre, and R. Denoyel, "Using pressure to provoke the structural transition of metal-organic frameworks," Angewandte Chemie International Edition 49, 7526–7529 (2010).
- ¹³N. Yanai, T. Uemura, M. Inoue, R. Matsuda, T. Fukushima, M. Tsujimoto, S. Isoda, and S. Kitagawa, "Guest-to-host transmission of structural changes for stimuli-responsive adsorption property," Journal of the American Chemical Society 134, 4501–4504 (2012).
- ¹⁴A. Modrow, D. Zargarani, R. Herges, and N. Stock, "The first porous MOF with photoswitchable linker molecules," Dalton transactions **40**, 4217–4222 (2011).
- ¹⁵A. Knebel, C. Zhou, A. Huang, J. Zhang, L. Kustov, and J. Caro, "Smart Metal-Organic Frameworks (MOFs): Switching Gas Permeation through MOF Membranes by External Stimuli," Chemical Engineering & Technology 41, 224–234 (2018).
- ¹⁶R. Kitaura, K. Seki, G. Akiyama, and S. Kitagawa, "Porous coordination-polymer crystals with gated channels specific for supercritical gases," Angewandte Chemie **115**, 444–447 (2003).
- ¹⁷C. Serre, F. Millange, C. Thouvenot, M. Nogues, G. Marsolier, D. Louër, and G. Férey, "Very large breathing effect in the first nanoporous chromium (III)-based solids: MIL-53

- or $Cr^{III}(OH) \cdot \{O_2C C_6H_4 CO_2\} \cdot \{HO_2C C_6H_4 CO_2H\}_x \cdot H_2O_y$," Journal of the American chemical society **124**, 13519–13526 (2002).
- ¹⁸D. Bousquet, F.-X. Coudert, A. G. Fossati, A. V. Neimark, A. H. Fuchs, and A. Boutin, "Adsorption induced transitions in soft porous crystals: An osmotic potential approach to multistability and intermediate structures," The Journal of chemical physics 138, 174706 (2013).
- ¹⁹F.-X. Coudert, M. Jeffroy, A. H. Fuchs, A. Boutin, and C. Mellot-Draznieks, "Thermodynamics of guest-induced structural transitions in hybrid organic-inorganic frameworks," Journal of the American Chemical Society 130, 14294–14302 (2008).
- ²⁰S. Lowell, J. E. Shields, M. A. Thomas, and M. Thommes, *Characterization of porous solids and powders: surface area, pore size and density*, Vol. 16 (Springer Science & Business Media, 2012).
- ²¹M. Thommes, K. Kaneko, A. V. Neimark, J. P. Olivier, F. Rodriguez-Reinoso, J. Rouquerol, and K. S. Sing, "Physisorption of gases, with special reference to the evaluation of surface area and pore size distribution (IUPAC Technical Report)," Pure and applied chemistry 87, 1051–1069 (2015).
- ²²G. Y. Chen, T. Thundat, E. Wachter, and R. Warmack, "Adsorption-induced surface stress and its effects on resonance frequency of microcantilevers," Journal of Applied Physics **77**, 3618–3622 (1995).
- ²³C. Ganser, G. Fritz-Popovski, R. Morak, P. Sharifi, B. Marmiroli, B. Sartori, H. Amenitsch, T. Griesser, C. Teichert, and O. Paris, "Cantilever bending based on humidity-actuated mesoporous silica/silicon bilayers," Beilstein Journal of Nanotechnology 7, 637–644 (2016).
- ²⁴H. P. Lang, M. K. Baller, R. Berger, C. Gerber, J. K. Gimzewski, F. Battiston, P. Fornaro, J.-P. Ramseyer, E. Meyer, and H.-J. Güntherodt, "An artificial nose based on a micromechanical cantilever array," Analytica Chimica Acta 393, 59–65 (1999).
- ²⁵Q. Zhao, J. W. Dunlop, X. Qiu, F. Huang, Z. Zhang, J. Heyda, J. Dzubiella, M. Antonietti, and J. Yuan, "An instant multi-responsive porous polymer actuator driven by solvent molecule sorption," Nature communications 5, 1–8 (2014).
- ²⁶D. Van Opdenbosch, G. Fritz-Popovski, W. Wagermaier, O. Paris, and C. Zollfrank, "Moisture-driven ceramic bilayer actuators from a biotemplating approach," Advanced Materials 28, 5235–5240 (2016).

- ²⁷P. Kowalczyk, C. Balzer, G. Reichenauer, A. P. Terzyk, P. A. Gauden, and A. V. Neimark, "Using in-situ adsorption dilatometry for assessment of micropore size distribution in monolithic carbons," Carbon 103, 263–272 (2016).
- ²⁸C. Balzer, R. T. Cimino, G. Y. Gor, A. V. Neimark, and G. Reichenauer, "Deformation of microporous carbons during N₂, Ar, and CO₂ adsorption: Insight from the density functional theory," Langmuir 32, 8265–8274 (2016).
- ²⁹L. J. D. Frink and F. van Swol, "Stress isotherms of porous thin materials: Theoretical predictions from a nonlocal density functional theory," Langmuir **15**, 3296–3301 (1999).
- ³⁰S. Dourdain, D. Britton, H. Reichert, and A. Gibaud, "Determination of the elastic modulus of mesoporous silica thin films by x-ray reflectivity via the capillary condensation of water," Applied Physics Letters 93, 183108 (2008).
- ³¹F. Huber, H. Lang, N. Backmann, D. Rimoldi, and C. Gerber, "Direct detection of a BRAF mutation in total RNA from melanoma cells using cantilever arrays," Nature nanotechnology 8, 125–129 (2013).
- ³²K. Mogilnikov and M. Baklanov, "Determination of Young's modulus of porous low-k films by ellipsometric porosimetry," Electrochemical and Solid State Letters 5, F29 (2002).
- ³³J. Prass, D. Müter, P. Fratzl, and O. Paris, "Capillarity-driven deformation of ordered nanoporous silica," Applied physics letters 95, 083121 (2009).
- ³⁴J. Samuel, C. J. Brinker, L. J. Douglas Frink, and F. van Swol, "Direct measurement of solvation forces in complex microporous media: A new characterization tool," Langmuir 14, 2602–2605 (1998).
- ³⁵E. Ustinov and D. Do, "Effect of adsorption deformation on thermodynamic characteristics of a fluid in slit pores at sub-critical conditions," Carbon **44**, 2652–2663 (2006).
- ³⁶A. Kolesnikov, N. Georgi, Y. A. Budkov, J. Mollmer, J. Hofmann, J. Adolphs, and R. Glaser, "Effects of enhanced flexibility and pore size distribution on adsorption-induced deformation of mesoporous materials," Langmuir 34, 7575–7584 (2018).
- ³⁷M. Vandamme, "Coupling between adsorption and mechanics (and vice versa)," Current Opinion in Chemical Engineering **24**, 12–18 (2019).
- ³⁸A. Y. Ben-Naim, Solvation thermodynamics (Springer Science & Business Media, 2013).
- ³⁹L. D. Landau and E. M. Lifshitz, Course of theoretical physics (Elsevier, 2013).
- ⁴⁰P. B. Balbuena, D. Berry, and K. E. Gubbins, "Solvation pressures for simple fluids in micropores," The Journal of Physical Chemistry **97**, 937–943 (1993).

- ⁴¹P. Tarazona, "Free-energy density functional for hard spheres," Physical Review A **31**, 2672 (1985).
- ⁴²W. A. Steele, *The interaction of gases with solid surfaces*, Vol. 3 (Pergamon, 1974).
- ⁴³W. A. Steele, "The physical interaction of gases with crystalline solids: I. Gas-solid energies and properties of isolated adsorbed atoms," Surface Science **36**, 317–352 (1973).
- ⁴⁴B. Derjaguin and N. Churaev, "Polymolecular adsorption and capillary condensation in narrow slit pores," Journal of Colloid and Interface Science **54**, 157–175 (1976).
- ⁴⁵D. Grégoire, C. Malheiro, and C. Miqueu, "Estimation of adsorption-induced pore pressure and confinement in a nanoscopic slit pore by a density functional theory," Continuum Mechanics and Thermodynamics **30**, 347–363 (2018).
- ⁴⁶A. Gil-Villegas, A. Galindo, P. J. Whitehead, S. J. Mills, G. Jackson, and A. N. Burgess, "Statistical associating fluid theory for chain molecules with attractive potentials of variable range," The Journal of chemical physics **106**, 4168–4186 (1997).
- ⁴⁷R. G. Horn and J. N. Israelachvili, "Direct measurement of structural forces between two surfaces in a nonpolar liquid," The Journal of Chemical Physics **75**, 1400–1411 (1981).
- ⁴⁸J. Landers, G. Y. Gor, and A. V. Neimark, "Density functional theory methods for characterization of porous materials," Colloids and Surfaces A: Physicochemical and Engineering Aspects **437**, 3–32 (2013).
- ⁴⁹G. Y. Gor and A. V. Neimark, "Adsorption-induced deformation of mesoporous solids," Langmuir **26**, 13021–13027 (2010).
- ⁵⁰A. V. Neimark and P. I. Ravikovitch, "Capillary condensation in MMS and pore structure characterization," Microporous and Mesoporous Materials **44**, 697–707 (2001).
- ⁵¹G. Y. Gor, C. D. Dobrzanski, and A. Emelianova, "Thermodynamic fingerprints of nanoporous materials on the fluids confined in their pores," Soft Matter and Biomaterials on The Nanoscale: The WSPC Reference on Functional Nanomaterials - Part I (In 4 Volumes) 20, 227 (2020).
- ⁵²It can be seen as a pore-load modulus³³, i.e. the effective elastic constant reflecting the material response due to the adsorption-induced stress. The detailed discussion can be found in the Ref.1.
- ⁵³P. I. Ravikovitch and A. V. Neimark, "Density functional theory model of adsorption on amorphous and microporous silica materials," Langmuir **22**, 11171–11179 (2006).

- ⁵⁴G. Y. Gor and A. V. Neimark, "Adsorption-induced deformation of mesoporous solids: Macroscopic approach and density functional theory," Langmuir **27**, 6926–6931 (2011).
- ⁵⁵A. L. Kolesnikov, Y. A. Budkov, and G. Y. Gor, "Adsorption-induced deformation of mesoporous materials with corrugated cylindrical pores," The Journal of Chemical Physics 153, 194703 (2020).
- ⁵⁶A. L. Kolesnikov, Y. A. Budkov, J. Mollmer, M. G. Kiselev, and R. Glaser, "Metalorganic framework breathing in the electric field: A theoretical study," The Journal of Physical Chemistry C 123, 10333–10338 (2019).
- ⁵⁷C. J. Gommes, "Adsorption, capillary bridge formation, and cavitation in SBA-15 corrugated mesopores: a Derjaguin–Broekhoff–de Boer analysis," Langmuir **28**, 5101–5115 (2012).
- ⁵⁸C. J. Gommes, H. Friedrich, M. Wolters, P. E. d. Jongh, and K. P. d. Jong, "Quantitative characterization of pore corrugation in ordered mesoporous materials using image analysis of electron tomograms," Chemistry of Materials 21, 1311–1317 (2009).
- ⁵⁹C. J. Gommes, H. Friedrich, P. E. De Jongh, and K. P. De Jong, "2-Point correlation function of nanostructured materials via the grey-tone correlation function of electron tomograms: A three-dimensional structural analysis of ordered mesoporous silica," Acta materialia 58, 770–780 (2010).
- ⁶⁰T. Hofmann, D. Wallacher, J. Perlich, S. Koyiloth Vayalil, and P. Huber, "Formation of periodically arranged nanobubbles in mesopores: capillary bridge formation and cavitation during sorption and solidification in an hierarchical porous SBA-15 matrix," Langmuir 32, 2928–2936 (2016).
- ⁶¹O. K. Krasilnikova, B. P. Bering, V. V. Serpinskii, and M. M. Dubinin, "Deformation of zeolite CaNaX during xenon adsorption," Bulletin of the Academy of Sciences of the USSR, Division of chemical science 26, 1099–1101 (1977).
- ⁶²A. Emelianova, M. A. Maximov, and G. Y. Gor, "Solvation pressure in spherical mesopores: Macroscopic theory and molecular simulations," AIChE Journal **67**, e16542 (2021).
- ⁶³W. Haiss, "Surface stress of clean and adsorbate-covered solids," Reports on Progress in Physics **64**, 591 (2001).
- ⁶⁴G. Y. Gor and N. Bernstein, "Adsorption-induced surface stresses of the water/quartz interface: Ab initio molecular dynamics study," Langmuir 32, 5259–5266 (2016).

- ⁶⁵A. L. Kolesnikov, Y. A. Budkov, and G. Y. Gor, "Density Functional Theory Model for Adsorption-Induced Deformation of Mesoporous Materials with Nonconvex Pore Geometry," The Journal of Physical Chemistry C 124, 20046–20054 (2020).
- ⁶⁶S. Jun, S. H. Joo, R. Ryoo, M. Kruk, M. Jaroniec, Z. Liu, T. Ohsuna, and O. Terasaki, "Synthesis of new, nanoporous carbon with hexagonally ordered mesostructure," Journal of the American Chemical Society **122**, 10712–10713 (2000).
- ⁶⁷D. Henderson, Fundamentals of inhomogeneous fluids (CRC Press, 1992).
- ⁶⁸Y. Rosenfeld, "Free-energy model for the inhomogeneous hard-sphere fluid mixture and density-functional theory of freezing," Physical review letters **63**, 980 (1989).
- ⁶⁹J.-P. Hansen and I. R. McDonald, *Theory of simple liquids* (Elsevier, 1990).
- ⁷⁰V. Yelpo, V. Cornette, J. P. Toso, and R. H. López, "Characterization of nanostructured carbon CMK-3 by means of Monte Carlo simulations," Carbon **121**, 106–113 (2017).
- ⁷¹M. Chen, B. Coasne, R. Guyer, D. Derome, and J. Carmeliet, "Molecular simulation of sorption-induced deformation in atomistic nanoporous materials," Langmuir 35, 7751–7758 (2019).
- ⁷²L. Ludescher, R. Morak, S. Braxmeier, C. Balzer, F. Putz, S. Busch, N. Hüsing, G. Reichenauer, G. Y. Gor, and O. Paris, "Adsorption-induced deformation of hierarchical organised carbon materials with ordered, non-convex mesoporosity," Molecular Physics, e1894362 (2021).
- ⁷³A. Grosman and C. Ortega, "Influence of elastic strains on the adsorption process in porous materials: An experimental approach," Langmuir **25**, 8083–8093 (2009).
- ⁷⁴M. Bossert, A. Grosman, I. Trimaille, C. Nous, and E. Rolley, "Stress or strain does not impact sorption in stiff mesoporous materials," Langmuir 36, 11054–11060 (2020).
- ⁷⁵W. Curtin and N. Ashcroft, "Weighted-density-functional theory of inhomogeneous liquids and the freezing transition," Physical review A **32**, 2909 (1985).
- ⁷⁶F.-X. Coudert, "Responsive metal-organic frameworks and framework materials: under pressure, taking the heat, in the spotlight, with friends," Chemistry of Materials **27**, 1905–1916 (2015).
- ⁷⁷A. V. Neimark, F.-X. Coudert, A. Boutin, and A. H. Fuchs, "Stress-based model for the breathing of metal- organic frameworks," The journal of physical chemistry letters 1, 445–449 (2010).

- ⁷⁸A. Boutin, M.-A. Springuel-Huet, A. Nossov, A. Gedeon, T. Loiseau, C. Volkringer, G. Férey, F.-X. Coudert, and A. H. Fuchs, "Breathing transitions in MIL-53 (Al) metalorganic framework upon xenon adsorption," Angewandte Chemie 121, 8464–8467 (2009).
- ⁷⁹S. Watanabe, H. Sugiyama, H. Adachi, H. Tanaka, and M. T. Miyahara, "Free energy analysis for adsorption-induced lattice transition of flexible coordination framework," The Journal of chemical physics 130, 164707 (2009).
- ⁸⁰A. Ghysels, L. Vanduyfhuys, M. Vandichel, M. Waroquier, V. Van Speybroeck, and B. Smit, "On the thermodynamics of framework breathing: A free energy model for gas adsorption in MIL-53," The Journal of Physical Chemistry C 117, 11540–11554 (2013).
- ⁸¹F.-X. Coudert, C. Mellot-Draznieks, A. H. Fuchs, and A. Boutin, "Double structural transition in hybrid material MIL-53 upon hydrocarbon adsorption: The thermodynamics behind the scenes," Journal of the American Chemical Society **131**, 3442–3443 (2009).
- ⁸²F.-X. Coudert, C. Mellot-Draznieks, A. H. Fuchs, and A. Boutin, "Prediction of breathing and gate-opening transitions upon binary mixture adsorption in metal- organic frameworks," Journal of the American Chemical Society 131, 11329–11331 (2009).
- ⁸³L. J. Dunne and G. Manos, "Statistical mechanics of binary mixture adsorption in metalorganic frameworks in the osmotic ensemble," Philosophical Transactions of the Royal Society A: Mathematical, Physical and Engineering Sciences 376, 20170151 (2018).
- ⁸⁴P. Kowalczyk, A. Ciach, and A. V. Neimark, "Adsorption-induced deformation of microporous carbons: Pore size distribution effect," Langmuir **24**, 6603–6608 (2008).
- ⁸⁵P. Schiller, T. Bier, M. Wahab, and H.-J. Mögel, "Mesoscopic model of volume changes due to moisture variations in porous materials," Colloids and Surfaces A: Physicochemical and Engineering Aspects 327, 34–43 (2008).
- ⁸⁶M. Chen, B. Coasne, R. Guyer, D. Derome, and J. Carmeliet, "A Poromechanical Model for Sorption Hysteresis in Nanoporous Polymers," The Journal of Physical Chemistry B 124, 8690–8703 (2020).
- ⁸⁷M. Chen, B. Coasne, R. Guyer, D. Derome, and J. Carmeliet, "Role of hydrogen bonding in hysteresis observed in sorption-induced swelling of soft nanoporous polymers," Nature communications 9, 1–7 (2018).
- ⁸⁸K. A. Cychosz and M. Thommes, "Progress in the physisorption characterization of nanoporous gas storage materials," Engineering 4, 559–566 (2018).

- ⁸⁹E. Kierlik, P. Monson, M. Rosinberg, L. Sarkisov, and G. Tarjus, "Capillary condensation in disordered porous materials: Hysteresis versus equilibrium behavior," Physical review letters 87, 055701 (2001).
- ⁹⁰P. A. Monson, "Understanding adsorption/desorption hysteresis for fluids in mesoporous materials using simple molecular models and classical density functional theory," Microporous and Mesoporous Materials 160, 47–66 (2012).
- ⁹¹A. Svidrytski, D. Hlushkou, M. Thommes, P. A. Monson, and U. Tallarek, "Modeling the impact of mesoporous silica microstructures on the adsorption hysteresis loop," The Journal of Physical Chemistry C 124, 21646–21655 (2020).
- ⁹²D. Bangham and N. Fakhoury, "The swelling of charcoal. Part I. Preliminary experiments with water vapour, carbon dioxide, ammonia, and sulphur dioxide," Proceedings of the Royal Society of London. Series A, Containing Papers of a Mathematical and Physical Character 130, 81–89 (1930).
- ⁹³D. Bangham, N. Fakhoury, and A. Mohamed, "The swelling of charcoal. Part II. Some factors controlling the expansion caused by water, benzene and pyridine vapours," Proceedings of the Royal Society of London. Series A, Containing Papers of a Mathematical and Physical Character 138, 162–183 (1932).
- ⁹⁴D. Bangham, N. Fakhoury, and A. Mohamed, "The swelling of charcoal. Part III. Experiments with the lower alcohols," Proceedings of the Royal Society of London. Series A-Mathematical and Physical Sciences 147, 152–175 (1934).
- ⁹⁵G. Y. Gor and N. Bernstein, "Revisiting Bangham's law of adsorption-induced deformation: changes of surface energy and surface stress," Physical Chemistry Chemical Physics 18, 9788–9798 (2016).
- ⁹⁶G. El Tabbal, P. Dangla, M. Vandamme, M. Bottoni, and S. Granet, "Modelling the drying shrinkage of porous materials by considering both capillary and adsorption effects," Journal of the Mechanics and Physics of Solids 142, 104016 (2020).
- ⁹⁷I. Maruyama, J. Rymeš, M. Vandamme, and B. Coasne, "Cavitation of water in hardened cement paste under short-term desorption measurements," Materials and Structures 51, 1–13 (2018).
- ⁹⁸V. Baroghel-Bouny, M. Mainguy, T. Lassabatere, and O. Coussy, "Characterization and identification of equilibrium and transfer moisture properties for ordinary and high-performance cementitious materials," Cement and concrete research 29, 1225–1238 (1999).

- ⁹⁹A. V. Neimark and I. Grenev, "Adsorption-Induced Deformation of Microporous Solids: A New Insight from a Century-Old Theory," The Journal of Physical Chemistry C 124, 749–755 (2019).
- ¹⁰⁰M. M. Dubinin, "Physical adsorption of gases and vapors in micropores," in *Progress in surface and membrane science*, Vol. 9 (Elsevier, 1975) pp. 1–70.
- ¹⁰¹R. A. Guyer and H. A. Kim, "Theoretical model for fluid-solid coupling in porous materials," Physical Review E **91**, 042406 (2015).
- ¹⁰²S. Bakhshian, Z. Shi, M. Sahimi, T. T. Tsotsis, and K. Jessen, "Image-based modeling of gas adsorption and deformation in porous media," Scientific reports 8, 1–12 (2018).
- ¹⁰³T. Zhou, K. Ioannidou, E. Masoero, M. Mirzadeh, R. J.-M. Pellenq, and M. Z. Bazant, "Capillary stress and structural relaxation in moist granular materials," Langmuir 35, 4397–4402 (2019).
- ¹⁰⁴K. Ioannidou, K. J. Krakowiak, M. Bauchy, C. G. Hoover, E. Masoero, S. Yip, F.-J. Ulm, P. Levitz, R. J.-M. Pellenq, and E. Del Gado, "Mesoscale texture of cement hydrates," Proceedings of the National Academy of Sciences 113, 2029–2034 (2016).
- 105D. J. Korteweg, "Sur la forme que prennent les équations du mouvements des fluides si l'on tient compte des forces capillaires causées par des variations de densité considérables mais connues et sur la théorie de la capillarité dans l'hypothèse d'une variation continue de la densité," Archives Néerlandaises des Sciences exactes et naturelles 6, 1–24 (1901).
- ¹⁰⁶D. M. Anderson, G. B. McFadden, and A. A. Wheeler, "Diffuse-interface methods in fluid mechanics," Annual review of fluid mechanics **30**, 139–165 (1998).
- ¹⁰⁷R. F. Feldman, "Sorption and length change scanning isotherms of methanol and water on hydrated Portland cement," in *Proc. 5th Int. Symp. Chem. Cement, Tokyo, 1968* (1968).
- ¹⁰⁸M. B. Pinson, E. Masoero, P. A. Bonnaud, H. Manzano, Q. Ji, S. Yip, J. J. Thomas, M. Z. Bazant, K. J. Van Vliet, and H. M. Jennings, "Hysteresis from multiscale porosity: Modeling water sorption and shrinkage in cement paste," Physical Review Applied 3, 064009 (2015).